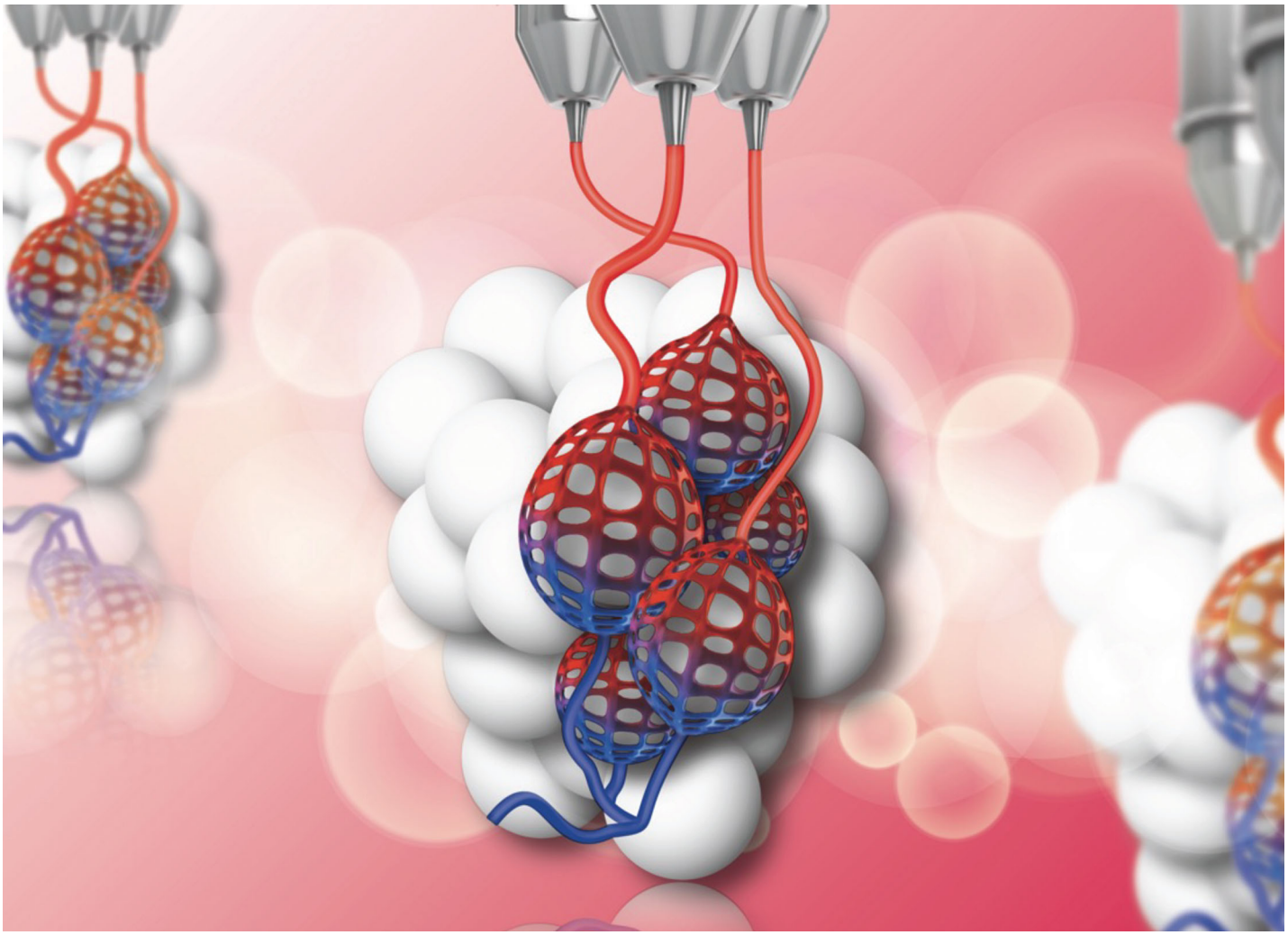

Showcasing a review of the recent advancements of new materials and 3D printing techniques in biomedical applications by Dr Hiroyuki Tetsuka and Assistant Professor Su Ryon Shin of Brigham and Women's Hospital, Harvard Medical School, USA.

Materials and technical innovations in 3D printing in biomedical applications

A comparative study of 3D printing materials and technologies, with respect to the 3D printing parameters, has been provided towards selecting a suitable application-based 3D printing methodology.

As featured in:

See Hiroyuki Tetsuka and Su Ryon Shin, *J. Mater. Chem. B*, 2020, **8**, 2930.

ROYAL SOCIETY OF CHEMISTRY

rsc.li/materials-b

Registered charity number: 207890

Journal of Materials Chemistry B

ROYAL SOCIETY OF CHEMISTRY

REVIEW

View Article Online
View Journal | View Issue

Cite this: J. Mater. Chem. B, 2020, 8, 2930

Materials and technical innovations in 3D printing in biomedical applications

Hiroyuki Tetsuka [ab] and Su Ryon Shin *[a]

Received 6th January 2020,
Accepted 7th March 2020

DOI: 10.1039/d0tb00034e

rsc.li/materials-b

3D printing is a rapidly growing research area, which significantly contributes to major innovations in various fields of engineering, science, and medicine. Although the scientific advancement of 3D printing technologies has enabled the development of complex geometries, there is still an increasing demand for innovative 3D printing techniques and materials to address the challenges in building speed and accuracy, surface finish, stability, and functionality. In this review, we introduce and review the recent developments in novel materials and 3D printing techniques to address the needs of the conventional 3D printing methodologies, especially in biomedical applications, such as printing speed, cell growth feasibility, and complex shape achievement. A comparative study of these materials and technologies with respect to the 3D printing parameters will be provided for selecting a suitable application-based 3D printing methodology. Discussion of the prospects of 3D printing materials and technologies will be finally covered.

1. Introduction

Since the invention of the stereolithography (SLA) method and the creation of the first three-dimensional (3D) printed object during the 1980s by Hull,[1,2] 3D printing has been adopted in various areas such as engineering, manufacturing, medicine, and education, in a widespread way. Now, over the past 40 years, the technology has been evolving, allowing researchers to create 3D objects with complex geometries that were previously difficult to make using conventional fabrication techniques and invent innovative systems.[3–10] The progress in 3D printing enabled researchers to create complex objects, biomimetic tissue constructs, autonomous soft robots, and customized drug delivery systems, and facilitated the development of system designs with higher resolution and more precise control by combining multi-material design, machine learning, and topological optimization algorithms.[11–29]

Fig. 1 summarizes the technical innovations and materials in the history of 3D printing. Conventional 3D printing processes, where 3D objects are constructed by adding layers of materials onto a planar surface as a line or a point, include material extrusion, vat photopolymerization, material or binder jetting, powder bed fusion, sheet lamination, and directed energy deposition.[5] By 1986, Hull had successfully commercialized an SLA-based 3D printer, which is a refined version of the first printer. SLA adopts a vat photopolymerization process to convert a liquid plastic (typically acrylate) into a solid object, through a laser scan of liquid photocurable material.[1,2] Later, other inventors began to create alternatives to Hull's UV light-based system. In 1989, following Hull's invention, Deckard developed an alternative method of 3D printing, called the selective laser sintering (SLS) method.[30] In SLS, a laser is used as the power source to fuse or sinter powdered materials, typically made of plastic, metal, ceramic, and glass, to create solid 3D objects in a layer-by-layer manner. The powdered materials vary depending on the targeted 3D object.

Another important 3D printing method, fused deposition modelling (FDM), was invented by Crump in 1988.[31] FDM, one of the material extrusion technologies, uses a thermoplastic filament feed into a heated nozzle to deposit filaments on a printing substrate in a layer-by-layer fashion. It extrudes heated plastic filaments through a nozzle to build up objects. FDM-based 3D printers have pioneered a new way of manufacturing products since their invention and provided a new method of creating prototypes at a lower cost.

SLA was the first system of additive manufacturing (AM) with high resolution and high printing speed, but nowadays cost-effective FDM is the most widely used 3D printing method. Despite the rapid advancement in AM, its low printing speed, scalability, and quality have hampered the adaptation of 3D printing in large-scale manufacturing applications. Nevertheless, 3D printing capable of printing complex 3D objects with high customizability has attracted the interest of many

[a] Division of Engineering in Medicine, Department of Medicine, Brigham and Women's Hospital, Harvard Medical School, 65 Lansdowne Street, Cambridge, Massachusetts, 02139, USA. E-mail: sshin4@bwh.harvard.edu
[b] Future Research Department, Toyota Research Institute of North America, Toyota Motor North America, 1555 Woodridge Avenue, Ann Arbor, Michigan, 48105, USA. E-mail: hiroyuki.tetsuka@toyota.com

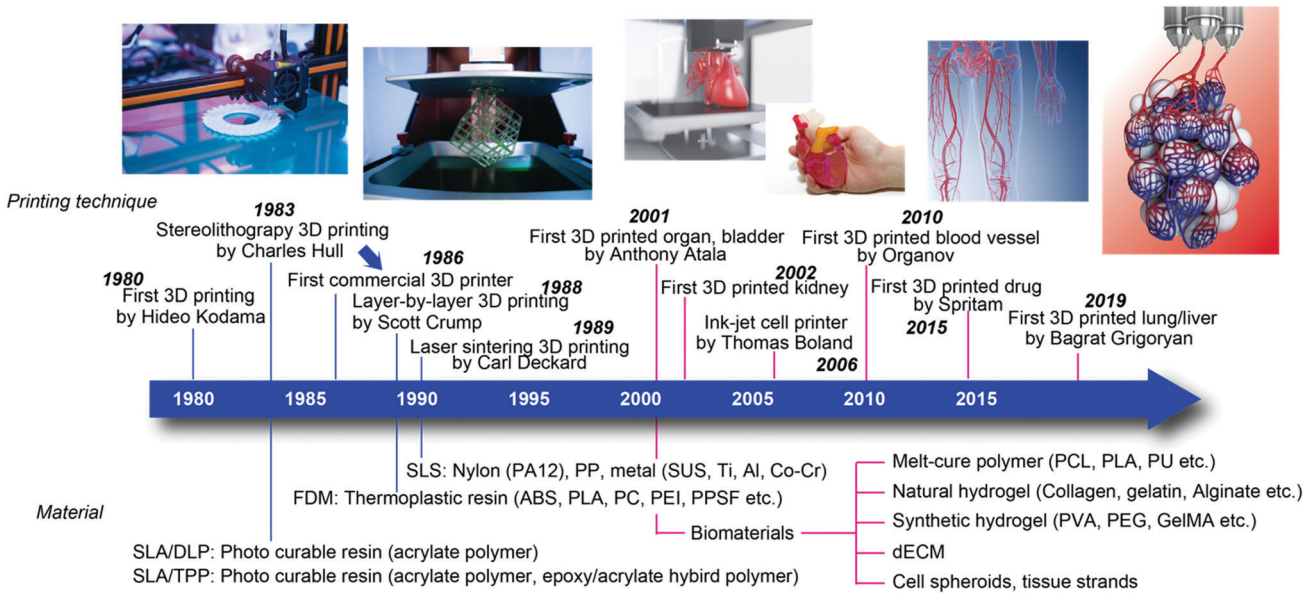

Fig. 1 Important events in the history of 3D printing.

researchers, because its features are extremely useful for rapid prototyping, creating concept models, and manufacturing end-products ready to be sent to the market. Moreover, recent developments in machine learning-based processes, computer-aided design (CAD) software, and in novel materials, ranging from plastic and metals to ceramics and even food products, are further expanding the stage for 3D printing.

Medical researchers discovered that even complex parts of the human body can be created by using biomaterials as inks for 3D printing in the same way. Many advantages of 3D printing in biomedical applications are paving the way for possible medical solutions such as transplantation of human tissues or organs for regenerative medicine, and the 3D printing of human tissues and organs is now an emerging research topic. In 2001, for the first time, the transplantation of a 3D printed organ, a bladder, into a patient was reported by Atala. In order to fabricate the bladder, the researchers used a dome-shaped scaffold the size of a human bladder constructed from a biodegradable polymer and then coated the patient's own bladder cells layer-by-layer on it using a 3D printer. Two different types of cells used for bioinks were deposited on the scaffold, with urothelial cells on the inside and muscle cells on the outer surface.[32] However, the structure of Atala's bladder was quite simple. For the fabrication of other complex organs such as the heart and liver, researchers needed a method to mimic the vascular networks for keeping the organs alive.

In 2004, Forgacs *et al.* used a 3D printer to create tubular structures toward the fabrication of blood vessels and then vascular networks. They constructed 3D biological hollow tubes by culturing cells on the outer surface of 3D printed hollow tubes.[32] Their printer contained three print heads that deposited bioinks onto a gelatin sheet serving as the extracellular matrix (ECM). Until 2010, this technology was the basis for the 3D bioprinting company, Organovo. For a decade, 3D bioprinting has been developed and then applied in the fabrication of various artificial biological tissue constructs[33–40] for various biomedical applications such as tissue regeneration.[41–44] 3D bioprinting has also been widely used in the fabrication of biomimetic tissue models for studying the pathogenesis of various diseases, identifying and optimizing potential drugs, and inventing useful novel medical applications, because it has emerged as a promising technology to create complex tailor-made biological constructs with desired physical and biological properties and is rapidly growing.

In this review, we introduce and review recent advancements of new materials and 3D printing techniques developed to address the unfulfilled needs of the conventional 3D printing methodologies, especially in biomedical applications, such as printing speed, cell growth feasibility, and complex shape achievement. A comparative study of these materials and technologies with respect to the 3D printing parameters will be provided for selecting a suitable application-based 3D printing methodology. Discussion of the prospects of 3D printing materials and technologies will be finally covered.

2. Conventional 3D printing methods for medical applications

Nozzle-based techniques, which deposit bioink in a layer-by-layer regime, have commonly been used as a 3D printing method in biomedical applications to create biological 3D constructs.

The primary 3D printing methods for medical applications (inkjet-based, extrusion-based, and light-assisted methods) are illustrated in Fig. 2. The most used platform is based on the extrusion method, followed by the light-assisted and inkjet-based printing approaches.[45–65] All these 3D printing methods can print scaffolds for cell culture or biological constructs using

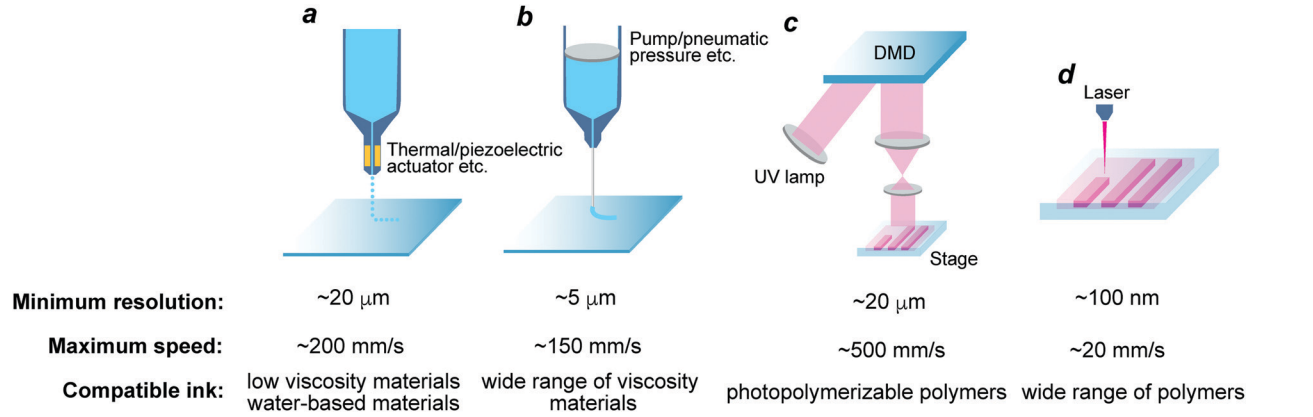

Fig. 2 Schematic illustration of the primary types of 3D printing techniques. (a) Inkjet-based 3D printing method. (b) Extrusion-based 3D printing method. (c) Dynamic optical projection stereolithography (DOPsL) 3D printing method. (d) Two-photon polymerization (TPP) 3D printing method.

cell-laden bioinks. However, there are some differences in the printing resolution, materials, speed, and mechanism among these methods. Sections 2.1–2.3 summarize each feature.

2.1 Inkjet-based 3D printing method

The inkjet-based method is presented in Fig. 2a. The first inkjet bioprinters were modified versions of commercially available benchtop 2D inkjet printers where a few picoliter droplets of bioink composed of biomaterials or cell mixtures in the cartridge are dispensed on an electronically controlled stage to control the *z*-axis. In an inkjet-based system, multiple actuation mechanisms are used, such as thermal, piezoelectric, electromagnetic, electrostatic, and acoustic, to produce a precise droplet.

Inkjet-based 3D printing methods have the potential to print at a speed of the order of 100 mm s^{-1} and a minimum resolution of 20–100 μm, typically 20 μm.[36,66] The nozzle diameter and the physical or chemical properties of the bioink determine the resolution of the printed constructs. Typically, higher printing resolution can be obtained with a smaller diameter of the nozzle heads. Inkjet-based methods generally require bioinks with a viscosity lower than 10 mPa s but offer a relatively fast printing speed compared to other techniques.[67] However, they provide low cell densities and decreased cell viability[68] and have problems caused by the inherent inability of the printing head to provide a continuous flow, limiting their capability to 3D print biological constructs compared to extrusion-based techniques.[69]

2.2 Extrusion-based 3D printing method

Extrusion-based 3D printing methods can control the flow of continuous bioinks and have been more widely employed than inkjet-based methods. A dispensing system, which uses pressure, mechanical, or solenoid valves, is adapted to drive the 3D printing system. Extrusion-based 3D printing methods can print cell-laden biomaterials as bioinks onto a target substrate or material in a layer-by-layer regime (Fig. 2b).

In extrusion-based methods, bioinks should have a viscosity in the range of 0.001–10 × 10^3 mPa s.[70] A wide variety of bioinks, *i.e.*, biomaterials, such as gelatin, alginate, hyaluronic acid (HA), and polyethylene glycol (PEG)-based hydrogels, decellularized extracellular matrix (dECM), and cell spheroids, are applicable, which makes extrusion-based methods highly advantageous compared to other printing methods.[71–74] However, they have limitations in printing speed and resolution. Their printing speed is in a wide range between 0.1 and 150 000 μm s^{-1}, typically 10–50 μm s^{-1}, and is the lowest among the three types of printing approaches.[70,75,76] In the case of a conventional single nozzle, it requires a long time to create large size tissue constructs with bioinks with good viability. A resolution of minimum 5–100 μm and generally over 100 μm has been reported.[70] This resolution makes it difficult to mimic the architecture of native components of the body such as microvessels, aligned myofibers, neuronal networks, *etc.* In comparison with inkjet-based 3D printing methods, extrusion-based 3D printing methods can handle bioinks with higher cell densities but provide lower printing speeds and resolution.[68]

2.3 Light-assisted 3D printing method

Compared to nozzle-based systems, light-assisted 3D printing can offer significant improvements in printing speed and resolution, accompanied by smooth features, different from inkjet-based and extrusion-based 3D printing methods. For light-assisted methods, bioinks with a wide range of viscosities, even fluids, are suitable. This enables us to use a larger range of biomaterials but these are restricted to photo-crosslinkable bioinks, typically composed of synthetic and natural biomaterials with photo-crosslinkable groups: gelatin methacryloyl (GelMA), poly(ethylene glycol) diacrylate (PEGDA) *etc.* In addition, to ensure an efficient light penetration depth, which affects the quality of the final constructs and the printing resolution, these biomaterials should be transparent against the light source used.

Two types of light-assisted 3D printing methods: the digital light processing (DLP) method and the two-photon polymerization (TPP) method, respectively, are mainly used to fabricate biological constructs.

2.3.1 DOPsL 3D printing method. The first light-assisted method, *i.e.* SLA, was developed by Hull. SLA is performed using a digital micromirror-array device (DMD) and controls an

array of up to several millions of micro-sized mirrors independently.[124,125] In this method, the construct is created in a layer-by-layer regime where one layer is fabricated and then the printing stage is lowered or raised to create a new layer. The entire layer is cured simultaneously. Based on this method, a dynamic optical projection stereolithography (DOPsL) system, which enables the rapid fabrication of complex 3D constructions, has been developed by Zhang *et al.* (Fig. 2c).

The DOPsL method provides a higher printing speed than other techniques, using a few million micromirror chips simultaneously, which makes it easy to fabricate large-scale complex constructs with submicron resolution. The printing speed reaches 500 mm s^{-1} and the printing resolution is as low as $\sim$10 μm.[126–128] This superior performance enabled researchers to build complex constructs: complex tissue constructs with fractal geometries, microfluidic mixing chambers, high-precision microwells constructed with tuneable Poisson ratios, aligned cardiac scaffolds, vasculature networks, and liver microarchitectures.[40,103,129–135] The DOPsL method has also used a wide variety of photopolymerizable hydrogels: GelMA, PEGDA, glycidyl methacrylate hyaluronic acid (GMHA) *etc.*, but capable biomaterials are limited to materials that can be photopolymerized.

2.3.2 TPP 3D printing method. Another light-assisted method is the TPP 3D printing method, which was developed from SLA as a kind of laser-based direct-writing technique. A laser, typically a femtosecond laser, is used to polymerize the photo linkable monomers repeatedly and selectively to generate constructs (Fig. 2d).[136] A femtosecond laser can induce two-photon absorption, which is the basic mechanism of the TP method. In a two-photon absorption process, the simultaneous absorption of the two photons induces the excitation of a molecule to a higher-energy electronic state. The probability that a molecule undergoes the two-photon absorption process relies on the square of the light intensity of the incident light.[137] The photons can be confined inside a voxel of size below 1 μm, which enables the printing resolution of TPP to reach only 100 nm.[136,138,139] Thus, TPP is an ideal platform for printing 3D objects with nanoscale to microscale features. The printing speed of the TPP method reaches 20 mm s^{-1}, which is much faster than those of the nozzle-based 3D printing methods.[140] TPP also accepts various polymers such as hydrogels, PEGDA, HA, collagen, bovine serum albumin, and laminin as bioinks.[141–145]

Although light-assisted 3D printing techniques have some limitations in the size of the printable constructs, they are now used in various tissue engineering applications and have great potential for fabricating complex 3D biological constructs within a short time.

3. Materials for 3D printing in biomedical applications

Bioinks used in 3D printing in biomedical applications are composed of biomaterials and cells. For 3D printing of biological constructs, biomaterials act as an ECM for cells, providing sufficient structural support and promising cellular attachment, to pattern the cells and the tissues. They also regulate cellular functions and behaviours. The ideal bioinks should not only be printable, but also be nontoxic and biocompatible to facilitate the biological behaviour of the seed cells or tissues. In order to sustain the functions of printed biological tissues, bioinks should fulfil certain characteristics required for each specific 3D printing technique.

3.1 Prerequisite parameters for biomaterials used in 3D printing

There are three main classes of biomaterials utilized in 3D printing: melt-cure polymers, hydrogels, and dECM. For biomaterials adopted in 3D printing, the most important prerequisite parameter is the biocompatibility. Basic cellular functions such as cell attachment and cell migration should be preserved for these biomaterials. For hydrogel-based biomaterials, photo-initiators are needed to crosslink the hydrogels by light exposure such as to UV and visible light, but these photoinitiators should also have little effect on the cell viability. It has been reported that some kinds of photo-initiators and monomers show cytotoxicity if left unreacted during the crosslinking process of hydrogels. The degradation rate of biomaterials should also be matched with the regeneration rate of tissue in order to offer sufficient structural support for cell activities to complete tissue regeneration.

The elasticity of hydrogels also affects the attachment and proliferation of cells, which depends on the glass transition state (T_g) of hydrogels.[161] Water-swelling causes a lower polymer glass transition and results in a decreased T_g, <37 °C. Subsequently, the hydrogels become a rubbery elastic state because the hydrogels are plasticized through the incorporation of excess water molecules. Therefore, the viscoelasticity of the hydrogels might be increased below T_g because the rearrangement of the polymer segments is restricted below T_g. Also, if hydrogels are sufficiently water-swollen during cell culturing, they can contain a large number of bioactive molecules that exist in cell culture media, resulting in improved cellular behaviours such as proliferation, differentiation, and elongation.

For biomaterials used in extrusion-based methods, another important parameter is non-Newtonian behaviour, determining the viscosity and flow behaviour of the biomaterials during dispensing. When pressure is applied to biomaterials during dispensing, they exhibit a variety of responses including shear thinning. The viscosity decreases with the increase in the shear rate. Yucel *et al.*[146] reported that the shear force reorganizes the conformation of polymer chains in the hydrogel and enhances the alignment of the polymer chains from a randomly-oriented conformation by reducing the viscosity of hydrogels during dispensing, *i.e.*, under shear stress (τ), called shear thinning. Shear-thinning has an impact on high molecular-weight biomaterials. This effect enables the easy dispensing of fluid materials under pressure and causes the fluidic biomaterials to restore to their gel state by relaxing their stress.

Because the fluidic event of biomaterials is initiated by the yield stress, which is an instantaneous stress, minimum stress

should be applied before they are dispensed. The yield stress (γ) affects the shear stress, and the structural network of biomaterials breaks when the applied shear force is greater than the yield stress. The yield stress also helps maintain the homogeneous distribution of cells within the bioink. The yield stress required for specific biomaterials can be estimated by extrapolating the flow curve at a low shear rate (μ) against zero shear rate. The Bingham or modified Bingham equation ($\tau = \tau_B + \mu_B\gamma$ or $\tau = \tau_{MB} + \mu_{MB}\gamma + C\gamma^2$), the simplest of the viscoelastic rheological models, can give the yield stress.[146,157] In the Bingham equations, changes in the yield stress by temperature, chemical concentration, and pH in biomaterials directly can be considered.

3.2 Appropriate biomaterial choice

Considering the requirements discussed in Section 3.1, the most important concern in 3D printing for biological constructs is the proper choice of biomaterials, which enables the design of target tissue scaffolds with desired chemical and physical properties. Table 1 summarizes some biomaterials used in different 3D printing techniques.

3.2.1 Melt-cure polymers. Melt-cure polymers have high mechanical strength and durability and can act as effective structural supports for tissues and cells. Typical melt-cure polymers are polycaprolactone (PCL), polylactic acid (PLA), and polyurethane (PU). Compared to PU and PLA, PCL is favourable as scaffolds because of its low melting point of $\sim$60 °C, which can reduce the temperature-induced cell damage. Several groups have demonstrated the use of PCL in a liver-on-a-chip, cartilage reconstruction, bone generation, muscle analogues, and vascular networks.[36,120,121,158] Similarly, PLA and PU have also been used in a heart-on-a-chip and neural tissues such as nerve grafts.[43,44,78,122,123] However, melt-cure polymers typically require either high process temperature or use of toxic solvents, which brings less cytocompatibility with cells compared to that of other biomaterials. In the printing process, the integration of these melt-cure polymers into cell-supportive hydrogels is also difficult.

3.2.2 Hydrogels. Hydrogels are one of the most important biomaterials since they inherently contain a large amount of water molecules and show good swelling features. Hydrogels can be categorized into two main classes: (1) naturally-derived hydrogels: collagen, gelatin, HA, alginate *etc.*, and (2) synthetically-derived hydrogels: PEG, poly(lactic-glycolic)acid (PLGA), PEGDA *etc.*

Hydrogels can form gel-like structures through physical, chemical, or enzymatic crosslinking.[159] Either a permanent or a reversible hydrogel is formed depending on the type of crosslinking state. Typically, irreversible permanent hydrogels are formed by introducing chemical bonds such as covalent bonds. Conversely, physical interactions such as hydrogen bonds and ionic forces produce reversible hydrogels. Although chemical crosslinking requires post-curing, the resultant permanent hydrogels show higher mechanical strength than physically cross-linked reversible hydrogels. However, hydrogels typically lack mechanical strength and shape fidelity compared to melt-cure polymers. In order to improve their mechanical strength and shape fidelity, the integration of hydrogels with melt-cure polymers such as PCL and PLGA has been investigated.

3.2.2.1 Natural hydrogels. The most commonly utilized natural hydrogels in 3D printing are gelatin, collagen, alginate, and HA.[160,161] These natural hydrogels are biodegradable and can promise native ECM-like environments required for cellular activities because they have similar mechanical properties and biological activities to the natural ECM. Natural hydrogels also show a defined structural feature and a distinct molecular weight, owing to their biological production methods.

Collagen, as the main component of the natural ECM and the most abundant protein in mammalian tissues, has been used in various applications such as a liver-on-a-chip and tissue constructs such as cartilage constructs.[43,93–95] Partial hydrolysis of collagen causes a helix-to-coil transition and thus produces another soluble protein-based polymer, gelatin. Gelatin exhibits lower antigenicity than collagen[123] and also undergoes gelation with a change in temperature. Although it usually remains in the gel state below 37 °C, an elevated temperature converts it to a liquid. This characteristic allowed it to be utilized as a sacrificial material for cells to construct organs-on-a-chip such as a liver-on-a-chip.[43] After cell incubation, only liquid gelatin was easily removed at decreased temperature, and then the cells remained. Gelatin can also be applied to produce a photopolymerizable hydrogel, GelMA, by the introduction of a methyl acrylate group as a synthetic part, which is a potential hydrogel for 3D printing. GelMA has been extensively utilized in various tissue engineering fields such as organ-on-a-chip, the construction of vascular networks, *etc.*[40,98,103,104]

Alginate and HA are also used to provide scaffolds for cartilage, chondrocytes, vascular networks with branch structures, skin tissue, and muscle constructs.[62,82–91] The physical properties of HA can be modified through chemical modifications by PEG, thiolate, guest–host supramolecular complexes *etc.* to enhance the printability and stability.[78] Alginate can be modified with RGD motifs to offer the mild 3D printing conditions needed for printing human pluripotent stem cells to generate mini-livers.[163,164] Other natural hydrogels, matrigel, fibrinogen, thrombin, chitosan, and agarose, are used in drug conversion in liver tissue,[89,92] skin and muscle constructs,[35,78,80,100] high-cell-density bioinks,[89] the reconstruction of cartilage and bones,[101] and the construction of vascular networks,[39,102] respectively. However, although natural hydrogels have been widely used for constructing various biological tissues, their main limitations are their relatively low mechanical strength, immunogenicity, and stability compared to synthetic hydrogels.

3.2.2.2 Synthetic hydrogels. In comparison with natural hydrogels, synthetic hydrogels have a well-defined structure, and their properties such as the degradation rate, mechanical strength, and structural characteristics can be more easily controlled reproducibly to enhance cell adhesion.[165] Since the late 1960s, the poly(2-hydroxyethyl methacrylate) (PHEMA) hydrogel has been widely used as an implantable material.

Table 1 Biomaterials used for 3D printing, classified according to the type of material

Biomaterials	Advantages	Disadvantages	Printing technique	Biomedical applications	Properties of biomedical parts	Cell viability in biomedical parts	Ref.
Melt-cure polymers							
PCL	High mechanical strength, highly durable	High process temperature, low cytocompatibility, need toxic solvents	Extrusion	Liver-on-a-chip, cartilage, bone, muscle	Low protein absorption and low optical transparency for an organ-on-a-chip (PCL scaffolds)	HepG2 and HUVEC (<95%)	43, 77 and 88
PLA				Heart-on-a-chip	Less absorption of hydrophobic drugs (PLA scaffolds)	Cardiomyocytes (high)	44
PU				Neural tissue, muscle tendon unit	High elasticity, and a stiffness the same as neural tissues (PU-based muscle tendon)	C2C12 (94%) and murine NSC (<95%)	78–81
Natural hydrogels							
Alginate	High cytocompatibility, native ECM-like microenvironment	Low mechanical strength	Inkjet, pneumatic extrusion, TPP, positive displacement extrusion	Cartilage, vascular construct	High compressive modulus of 20–70 kPa (alginate constructs)	ATDC5 (>85%)	62, 83–91 and 162
Matrigel			Pneumatic extrusion, TPP	Drug conversion on liver tissue	Capability of radiation exposure and anti-radiation drug treatment (matrigel channels)	HepG2 and M10 (high)	89 and 92
Collagen			Inkjet, pneumatic extrusion, TPP	Liver-on-a-chip, cartilage, heterogeneous tissue construct	High mechanical stability (~25 kPa compressive moduli) (collagen constructs)	Fibrochondrocyte (>90%)	43 and 93–95
Gelatin			Pneumatic extrusion, TPP, positive displacement extrusion	Liver-on-a-chip	High cytocompatibility for an organ-on-a-chip (gelatin channels)	HepG2 and HUVEC (<95%)	43, 80 and 96–98
Fibrinogen			Pneumatic extrusion	Skin, muscle	Deposition ability of large constructs (~100 cm^2) at a high speed (fibrin 3D scaffolds)	HaCaT keratinocytes and NIH/3T3 fibroblasts (good)	35 and 78
Thrombin			TPP	High cell density bioink	High printing resolution and a high cell density of 6×10^7 cells per mL (thrombin bioinks)	High for endothelial cells	89
Hyaluronan			Positive displacement extrusion	Vessel-like construct	Significantly higher shear storage moduli and superior cell growth and proliferation properties (hyaluronan constructs)	NIH/3T3 (>99%)	99
Chitosan			Extrusion	Cartilage, bone, skin	High elastic modulus of ~6 MPa (chitosan constructs)	L929 (>70%)	100 and 101
Agarose			Extrusion	Vascular network	Scaffold-free approach to construct a tubular structure (agarose templates)	Aortic smooth muscle cells (moderate)	39 and 102
Synthetic hydrogels							
GelMA	Moderate mechanical strength, good temperature sensitivity and photocrosslink ability	Low processability	Positive displacement extrusion, DOPsL	Liver-on-a-chip, vascular constructs	Superior formability and high strain moduli of 75–580 kPa (GelMA scaffolds)	3T3 and 10T1/2 (<80%)	40, 98, 103 and 104
PVA, PEG, PEGDA, PEGMA, PEGTA			Acoustic inkjet, positive displacement extrusion, SLA, DOPsL	Vascular constructs, cartilage	Good sacrificial layer ability (PVA–PEG-based hydrogels) Good elasticity tunability (PEGDA constructs)	NIH/3T3 (<80%)	102 and 105–108
Pluronic F-127, PLGA			Positive displacement extrusion	Vascular networks, cartilage, bone, muscle	Good printability, removability, and high elasticity of 2×10^4 Pa (Pluronic F-127-based inks)	HUVEC, 10T1/2, and HNDF (<80%)	77, 90 and 109

Table 1 (*continued*)

Biomaterials	Advantages	Disadvantages	Printing technique	Biomedical applications	Properties of biomedical parts	Cell viability in biomedical parts	Ref.
Hybrids							
Gelatin–GelMA, PEG–GelMA	Good mechanical strength, high cytocompatibility	—	Extrusion	Muscle, vascularized bone tissues	High compressive modulus and Young's modulus of ~5 kPa and high swelling ratio of ~35% (gelatin–GelMA constructs)	BMSC (<90%)	52, 110 and 111
PVA–gelatin–PEG			Extrusion	Cartilage	High (~10 kPa) and low (~100 kPa) moduli (PVA–gelatin–PEG constructs)	MSC (cell activity: >75%)	112
Pluronic F-127–alginate			Extrusion	Muscle, bone	High-resolution and long-term structural fidelity (Pluronic F-127–alginate constructs)	Chondrocyte and MSC (<80%)	62 and 113–116
PCL–alginate			Melt-plotting system, pneumatic extrusion	Scaffold for tissue engineering, cartilage, regenerative medicine	High Young's modulus of ~6 MPa (PCL–alginate constructs)	C20A4 (<65%)	80 and 117
PCL–PLGA–HA–gelatin–collagen			Melt-plotting system	Scaffold for tissue engineering, cartilage, muscle	Good printability and cytocompatibility (PCL–PLGA–gelatin constructs)	Hepatocyte and MC3T3-E1 (<90%)	118
PCL–fibrinogen–collagen			Electrospinning	Cartilage	High Young's modulus of ~1.7 MPa and good cytocompatibility (PCL–fibrinogen–collagen constructs)	Chondrocytes (<80%)	119
dECM	Retain native ECM components	Low processability	Pneumatic extrusion	Muscle, bone	Natural ECM microenvironment and low Young's modulus of ~1 kPa (dECM constructs)	hASCs, L6, and hTMSCs (<90%)	34, 120 and 168
Other cell spheroids, tissue strands	High cell density, no need for medium or supporting material	Long process time	Extrusion	Cartilage, vascular networks, nerve grafts	High Young's modulus of ~5 MPa (tissue strands constructs)	Chondrocytes (<75%)	39 and 121–123

However, currently, the most commonly used synthetic hydrogels are PEG and Pluronic F-127. PEGDA, a photo-crosslinkable hydrogel, is generated by the addition of photoinitiators.[166] PEGDA has been utilized in vascular construction[40,167] and in ear construction as a sacrificial material.[102,103] Other PEG-based hydrogels: poly-(ethylene glycol)methacrylate (PEGMA), poly(ethylene glycol)-tetra-acrylate (PEGTA) *etc.* have also been studied for reconstruction of bone and cartilage and vascular network construction.[59,77,90,105,106,108,109] Pluronic F-127, as a temperature-responsive hydrogel, can be converted to a liquid state at low temperatures. This feature allows its application as a sacrificial material for reconstruction of bone and cartilage, tissue engineering of muscle *etc.*, and construction of vascular channel networks.[59,77,90,109]

PVA can be photo-crosslinked to fabricate hydrogels and used in vascular tissue and cartilage constructs.[107,112] PVA hydrogels typically show a higher mechanical strength than most other synthetic hydrogels. They can also be copolymerized with PEG to produce biodegradable hydrogels, and their degradation rate is between that of the PVA hydrogel and the PEG hydrogel.

3.2.2.3 Hybrid hydrogels. While natural hydrogels possess better compatibility with cells, synthetic hydrogels have better processability such as printability and shape fidelity. To utilize these two advantages, hybrids of natural and synthetic hydrogels have been developed. In hybrid hydrogels, synthetic hydrogels enhance the mechanical strength while natural hydrogels retain the cell viability and functionality by offering an ECM microenvironment. A potential technique for fabricating hydrogel bioinks with both high printability and cytocompatibility is hybridization. Yin *et al.*[52] mixed gelatin with low-concentration GelMA and reversibly formed hydrogels by changing the bioink temperature to regulate the processability during 3D printing. The hybrid hydrogels showed higher cell compatibility than GelMA hydrogels. PEG and GelMA copolymerized hydrogels have been developed to tune their degradation rate and stiffness profiles.[111] The PEG–GelMA hydrogels exhibited improved cell viability and attachment compared to PEG hydrogels. Miao *et al.* developed a hybrid hydrogel composed of PVA–gelatin and PEG. They successfully controlled the modulus strength in the range of 10–100 kPa by changing the concentration of PVA and gelatin and the molecular weight of PVA. They have successfully utilized the hybrid hydrogel in cartilage regeneration.[112] Armstrong *et al.*[116] showed that hybrid hydrogels of alginate and Pluronic F-127 can be printed at high resolution using the extrusion method, and effectively crosslinked to produce constructs with high cytocompatibility and long-term structural fidelity. As alternative approaches, synthetic materials such as PCL and polydimethylsiloxane (PDMS) have been deposited as supportive scaffolds and mixed into natural hydrogels such as alginate, collagen, gelatin, and fibrinogen.[80,112,117–119,168,169]

Selected bioinks made from natural, synthetic, and hybrid hydrogels used for 3D printing are listed in Table 2. An appropriate biomaterial choice is made by considering a combination of the following factors: the used printing method, the target biological tissues and constructs, the cell types, and the biological processes to apply.[170,171] Regardless of the selected bioink, biomaterials have a quick crosslinking ability either in a chemical or physical manner in order to form a hydrogel network structure after or during the printing of 3D constructs. For instance, further development of water-soluble photoinitiators combined with high UV-visible absorption ability is urgent for 3D printing of hydrogels. Recently, Pawar *et al.*[172] developed highly efficient water-soluble nanoparticle-based UV curable inks, which allowed the 3D printing of hydrogels in an aqueous solution. The water-soluble nanoparticles were made from 2,4,6-trimethylbenzoyl-diphenylphosphine oxide (TPO). TPO can significantly absorb UV light from 385 to 420 nm and show an extinction coefficient as high as $\sim$680 M^{-1} cm^{-1}, which is over 300 times compared to that of commercially available water-soluble photoinitiators such as PIs (2.25 M^{-1} cm^{-1}). An n $\rightarrow$ π^* transition in the aroyl-phosphinoyl chromophore with strong conjugation between the phosphonyl group and the carbon

Table 2 Properties of selected bioinks made from natural, synthetic, and hybrid hydrogels

Biomaterials	Cell type	Cell density/viability	Printing condition	Ref.
Alginate 1%	NIH3T3, fibroblasts	5×10^6 mL^{-1} 90.8%	37 °C, extrusion	113, 114 and 147–149
Alginate 1–2%	Bone marrow stromal cells	2.5×10^6 mL^{-1} 95%	40 °C, extrusion	
Alginate 1–4%/GelMA 4.5%	HUVECs	3×10^6 mL^{-1} 80%	RT, 1–6 mm s^{-1}, 0.08 Pa s, coaxial needle extrusion	
Collagen 0.223%	Dermal fibroblasts	1×10^6 mL^{-1} 95%	37 °C, extrusion	110, 113, 114 and 147
Collagen 15 mg mL^{-1}/ alginate 0.1 g mL^{-1}	Primary chondrocytes	1×10^7 mL^{-1} 90%	RT, extrusion	
PEG 10%/GelMA 5%	NIH 3T3 fibroblasts	5×10^6 mL^{-1} 85%	RT, stereography	110
GelMA 5%	HUVECs, 10T1/2	40×10^6 mL^{-1} (HUVECs), 0.8×10^6 mL^{-1} (10T1/2s) 85%	RT, DLP	40, 113 and 150–154
GelMA 10–20%	HepG2	1.5×10^6 mL^{-1} 97%	27–37 °C, extrusion	
GelMA 10–20%	Articular cartilage	1.5×10^7 mL^{-1} 75–90%	37 °C, extrusion	
GelMA 3–20%/gellan gum 0–1.5%	NSCs	10–20 $\times 10^6$ mL^{-1}	RT, 475 mm min^{-1}, extrusion	
Gelatin 10–20%	Fibroblasts	5.9×10^5 mL^{-1} 91%	RT, laser direct-writing	97, 113, 114, 155 and 156
Pluronic PF127 20%/alginate 2%	C2C12	2×10^6 mL^{-1} 85%	37 °C, extrusion	62 and 113–115

atom of the adjacent carbonyl group is the origin of the strong, long wavelength absorption. Thus, the polymerization rate is magnificently enhanced. This enabled the 3D printing of hydrogels without adding any solvents.

3.2.3 dECM. The development of a novel biomaterial that enables the creation of complex biomimetic tissues is urgently needed. Most natural biomaterials cannot recreate the complexity of natural ECMs because they only have a single component from natural ECMs and lack important major components including proteoglycans, elastin, growth factors, and cell-binding glycoproteins such as laminin and fibronectin.[38] This is insufficient to mimic complex living tissues where a microenvironment with cell-to-cell connection and 3D cellular organization is typical. Consequently, researches have focused on dECM, which is derived from living tissues and organs for use in 3D printing as well as tissue engineering and regenerative medicine, as no natural or synthetic biomaterials can recapitulate all the features of natural ECMs.[173,174] In the decellularization process to fabricate dECM, all cellular components are removed from living tissues of organs through a combination of chemical, mechanical, and enzymatic treatments, which yield collagen while retaining important components of the native ECM. Perniconi *et al.* showed that cellular scaffolds can be explanted from mice and they effectively supported the formation of myofibers.[175] Furthermore, Pati *et al.* developed bioinks made of decellularized tissues derived from pepsin solubilized cartilage, adipose, and cardiac tissues. They also demonstrated the practicability of these tissue-specific dECMs as bioinks for use in nozzle-based 3D printing.[168] In fact, the constructs printed from bioinks made of these dECMs exhibited enhanced functionality of encapsulated mesenchymal stem cells derived from human inferior turbinate-tissue, human adipose-derived stem cells, and rat myoblasts compared to bioinks made of collagen. The fabrication of functional skeletal muscle constructs were also reported by other research groups using skeletal-derived dECM bioinks.[173] The significant increase in the osteogenic genes of human adipose-derived stem cells within dECM–PCL constructs manifested the effectiveness of dECM in bone regeneration compared to PCL scaffolds.[34] These studies imply the versatility of dECM in 3D printing for creating complex biological tissue constructs with a living tissue and organ-like microenvironment. However, dECM-based bioinks still have inferior printing formability such as shape fidelity, which should be addressed. dECM has also inherent ethical usage problems because of its origin.

Other biomaterials such as cell spheroids and tissue strands also have potential for replicating the functions and developing processes of native living tissues and organs. The direct 3D printing of cell spheroids- or tissue strand-laden bioinks has been reported through a scaffold-free method.[39]

4. Novel 3D printing techniques and materials

In this section, we introduce the recent advancements in novel 3D printing techniques and their related materials for biomedical applications. Interdisciplinary research lies between 3D printing techniques and advanced materials. Conventional 3D printing methods construct 3D objects by accumulating a layer. However, typically, these techniques lead to a step structure along the edges, called a stair-step effect. Limitations of speed, geometry, and surface quality exist in material layering methods. They also have difficulties creating 3D objects with both complexity and multi-functionality. The core problem is to improve the printability and formability of novel biomaterials without losing the superior features of the original material during the 3D printing process and the production of complex and multi-functional constructs.

4.1 Novel SLA and its materials

Recently, Kelly *et al.*[176] developed a novel 3D printing technique that uses computed tomography (CT), called computed axial lithography (CAL). The process of CAL was based on the image reconstruction procedure of CT, which is a technique widely used in medical imaging and non-destructive testing.[177,178] Recent developments in CT for use in cancer treatment provided an intensity-modulated radiation therapy (IMRT) method, which enables the targeted tumour areas of the patient's body to be exposed to a critical radiation dose in 3D.[179] Instead of the patient, a photoresponsive material is subjected to CT scans in CAL to obtain stair-step free, smooth, flexible, and complex 3D objects. The researchers used a viscous liquid, made from polymers with photocurable grafts and dissolved oxygen molecules, and designed the materials to react against a certain threshold of patterned light for solidification. The desired 3D shape was formed by projecting light onto a rotating cylinder of the liquid (Fig. 3a and b).

Using CAL, the formation of a centimetre-scale geometry can be completed in less than 1 min. It has the potential to produce a large array of geometries with a lateral size of up to $\sim$55 mm within a time range of 30 to 300 s. It is also possible to add new parts into an already existing object, *i.e.*, adding a handle to a metal screwdriver shaft, which is difficult to do using conventional 3D printing techniques. The printing materials do not have to be transparent. Even opaque 3D objects can be created using a dye molecule that absorbs visible light in a wide wavelength range except for the curing wavelength.

Grigoryan *et al.*[180] also developed versatile photopolymerizable hydrogels, which enable the fabrication of complex 3D objects for projection stereolithography. To date, it has been difficult to create complex 3D transport systems where organs transport blood *via* bio-physically and bio-chemically entangled complex vascular networks. To solve this problem, they established an intravascular and multivascular design using photopolymerizable hydrogels by incorporating a food dye as a biocompatible photoabsorber (Fig. 3b–k). Monolithic transparent hydrogels with intravascular 3D fluid mixers and bicuspid valves were produced in minutes using polyethylene glycol diacrylate with the food dye. Grigoryan *et al.* also introduced a hydrogel model of a lung-mimicking air sac with airways which enable the delivery of oxygen to the surrounding blood vessels. Successful implantation of bioprinted constructs including liver cells into mice was also demonstrated.

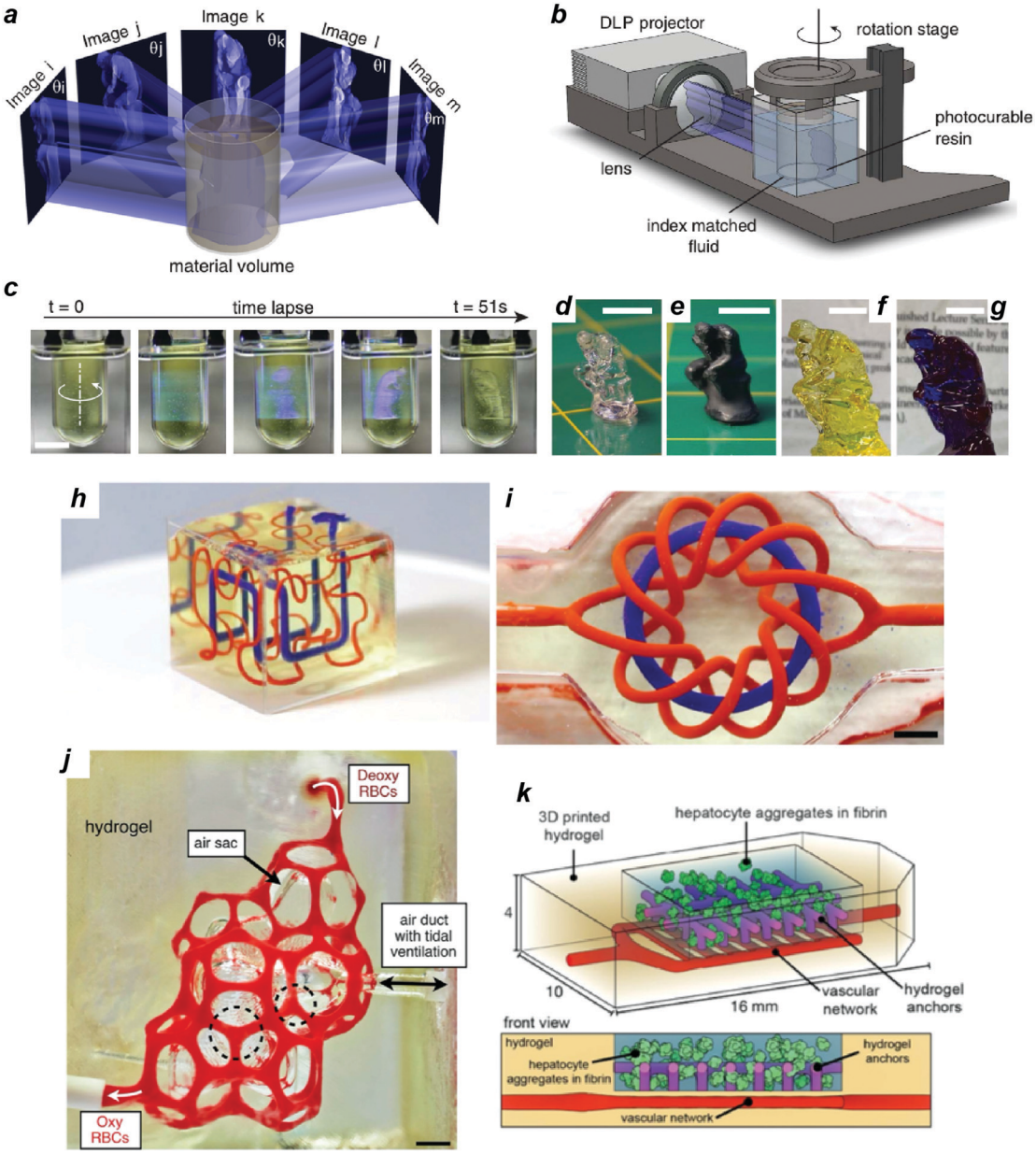

Fig. 3 (a) Underlying concept of CAL volumetric fabrication. (b) Schematic of the CAL system. (c) Sequential view of the build volume during CAL printing. (d) The object shown in (c) after rinsing away uncured resin. (e) The painted object for clarity from (d). (f) A larger 40 mm-tall version of the same geometry. (g) Opaque version of the geometry in (f). Scale bars are 10 mm. Reproduced with permission from ref. 176. Copyright 2019, AAAS. (h and i) Entangled vascular networks with vascularized alveolar model topologies. (j) Photograph of a printed hydrogel. The scale bar is 1 mm. (k) Engraftment of functional hepatic hydrogel carriers. Reproduced with permission from ref. 180. Copyright 2019, AAAS.

4.2 Multi-material 3D printing

Alternatively, Kang *et al.*[36] attempted to solve the challenges in producing 3D complex vascularized cellular networks using multi-material 3D printing systems. An integrated tissue-organ printer (ITOP) system that enables the fabrication of any shapes of human-scale tissue constructs was developed. This system was achieved by designing multi-dispensing systems for extruding and patterning multiple cell-laden hydrogels in a single construct: the poly(ε-caprolactone) polymer as a supporting construct and the Pluronic F-127 hydrogel as a sacrificial layer (Fig. 4a–c). They developed multiple materials and techniques: an optimized carrier material capable of positioning cells in the liquid form on distinct locations inside the 3D structure, sophisticated nozzle modules with a resolution as low as 2 μm for biomaterials and 50 μm for cells, and photo cross-linkable cell-laden hydrogels which have photocurable ability even after cell passage. They simultaneously printed an outer sacrificial acellular hydrogel mould that serves as a supporting layer. The lattice of microchannels permits the diffusion of nutrients and oxygen into the printed tissue constructs. The ITOP successfully generated various 3D constructs with multiple cell types and biomaterials and showed potential for fabricating various types

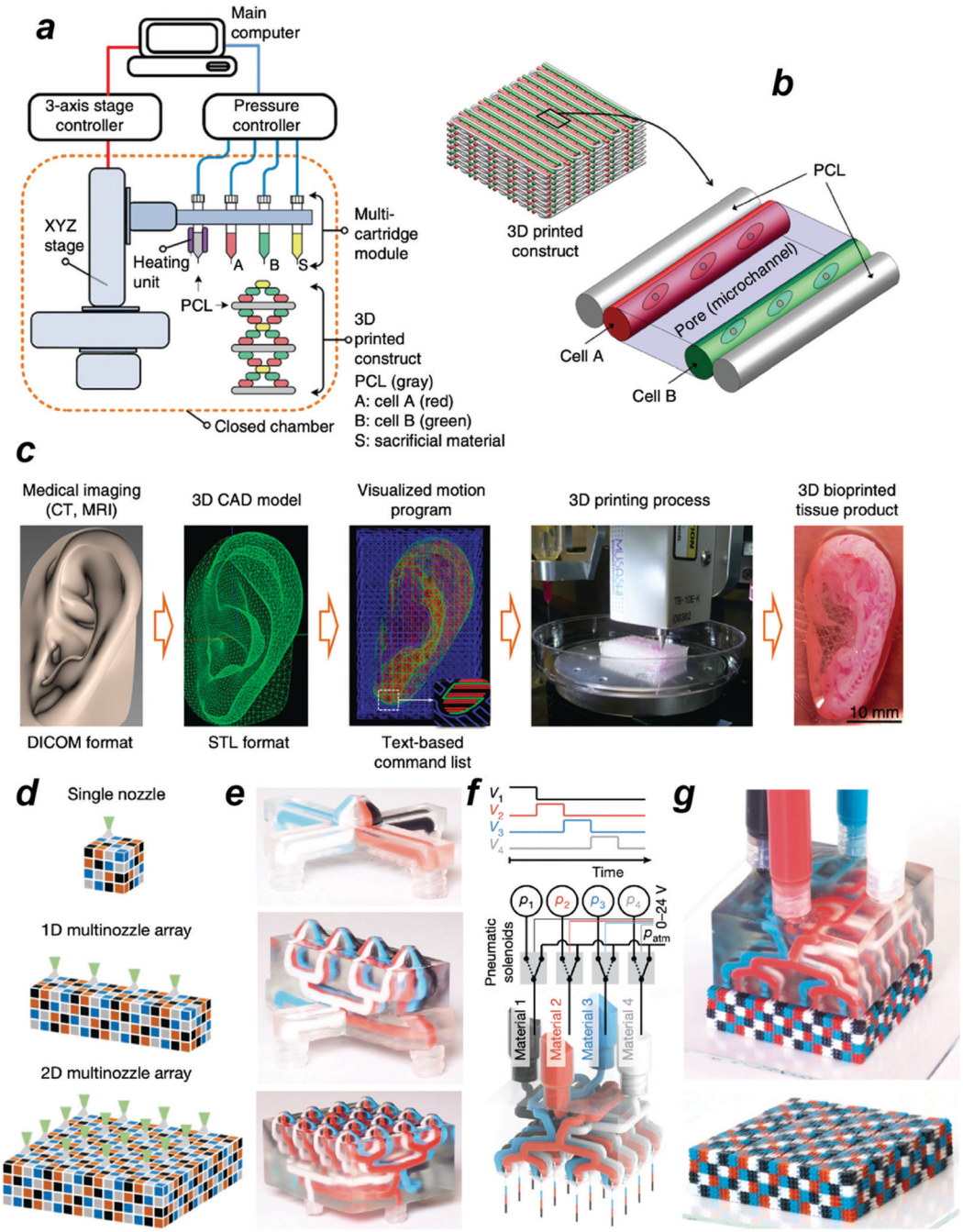

Fig. 4 (a) Schematic diagram of the ITOP system. (b) Illustration of basic patterning of a 3D architecture including multiple cell-laden hydrogels and the supporting PCL polymer. (c) CAD/CAM process for automated printing of 3D shapes imitating target tissues or organs. Reproduced with permission from ref. 36. Copyright 2019, AAAS. (d) Schematic of voxelated architectures printed using a single (0D) nozzle (top) and the 1D (middle) and 2D (bottom) MM3D printheads. (e) Photographs of the corresponding 0D, 1D and 2D four-material MM3D printheads. (f) Schematic of MM3D printhead operation. (g) Voxelated matter produced by MM3D printing using a 4 × 4-nozzle, four-material, 2D printhead. Reproduced with permission from ref. 181. Copyright 2019, Nature Publishing Group.

of vascularized tissues. The fabrication of novel organ-on-a-chip devices has also been demonstrated by Lind *et al.*,[44] who used a multi-material 3D bioprinting system. They designed biocompatible soft material-based functional multiple inks. High conductance and piezo-resistive characteristics of the inks induced self-assembly into physio-mimetic laminar cardiac tissues. The cardiac microphysiological devices were printed in a single step and applied to study the drug responses and the contractile mechanism of laminar cardiac tissues.

Furthermore, very recently, Skylar-Scott *et al.* developed an extrusion-based new multi-material printing technique that allows printing with up to eight different inks within a single

nozzle (Fig. 4d–g), called the multimaterial multinozzle 3D (MM3D) printing method.[181] They designed a printhead with a Y-shaped junction that enables the injection of multiple inks into a single nozzle, where each ink with different viscosities can be adjusted by varying the length of the ink channels. Precisely controlled high-speed pneumatic valves were utilized to achieve rapid and seamless switching between different inks, which drastically enhanced the printing speed. Complex 3D objects can be created in a fraction of the time of conventional extrusion-based techniques. Using the MM3D printing method, successful fabrication of 3D objects with a centimetre-scale, such as foldable origami structures and locomotive soft robots, composed of two alternating epoxy or silicon inks with different stiffnesses, was demonstrated within minutes at a speed of 10–40 mm s^{-1}.

4.3 Embedded 3D printing

Embedded 3D printing can provide another potential strategy for obtaining complex tissue-like constructs.[17,182–185] Initially, this method was demonstrated by Lewis *et al.*, who printed a 3D network of interconnected channels within a matrix composed of an acellular hydrogel and silicone using a viscoelastic, sacrificial ink.[182] After curing the matrices and removing the sacrificial ink, a 3D construct with an interconnected channel network was created. Embedded 3D printing involves extruding a viscoelastic ink into a reservoir with a high plateau shear elastic modulus, a low yield stress, and a photo-crosslinking ability. To meet these requirements, they developed a Pluronic F127 triblock copolymer with a hydrophobic poly(propylene oxide) segment and two hydrophilic poly(ethylene oxide) segments as a reservoir, though the chemical modification of the terminal hydroxyl groups of the hydrophilic poly(ethylene oxide) segments with diacrylate groups. Following Lewis's report, Burdrick *et al.* developed another embedded printing strategy based on supramolecular assembly of shear-thinning hydrogel inks through guest–host complexes, where a mixture of two different supramolecular hydrogels, adamantane modified HA serving as a guest and β-cyclodextrin modified HA serving as a host, was injected into a supporting hydrogel to create cell-laden 3D structures such as spirals and channels.[185–187] The formation of intermolecular guest–host non-covalent bonds between the adamantane modified HA and cyclodextrin modified HA allowed for the rapid formation of supramolecular assemblies. They also successfully extended this technique for use in biomedical applications such as drug delivery.

Recently, Luo *et al.* also developed a technique for generating complex, freeform, and liquid 3D architectures using formulated aqueous two-phase systems (ATPSs).[188] They used a polyethylene oxide matrix and an aqueous bioink made of a long carbohydrate molecule, called dextran (Fig. 5a and b). This system provides a several orders of magnitude lower tension compared to typical aqueous/organic phases, which suppressed the deformation of printed structures. The chemical interaction between hydrogen bonding within the polymers provided sufficient resistance against deformation and the aqueous-in-aqueous reconfigurable 3D architectures printed on the interface of the noncovalent membrane could stand for weeks. Tailor-made microconstructs with perfusable vascular networks were created by separately combining different cells with compartmentalized bioinks and matrices.

For use in embedded 3D printing, synthetic[183] and biopolymer[184,185] matrices with a viscoplastic response and self-healing features were further studied. Skylar-Scott *et al.*[189] developed organ building blocks (OBBs) composed of patient-specific-induced pluripotent stem cell (iPSC)-derived organoids and a technique called sacrificial writing into functional tissue (SWIFT). Thousands of OBBs were assembled into living matrices at a high cellular density and introduced into perfusable vascular channels. The OBB matrices exhibited the desired viscoelastic and self-healing behaviour to allow the rapid therapeutic-scale assembly of patient- and organ-specific tissues (Fig. 5c and d).

4.4 4D printing and materials

Tibbit *et al.*[44,190] originally introduced an idea for fabricating complex 3D objects that can react against an external environment stimulus, called the 4D printing method. They discovered a method for creating new design systems. The 4D printing method uses stimuli-responsive smart materials instead of conventional materials. This results in the formation of self-assembling and self-regulating constructs, which can change their shape upon external environmental stimuli.[3,190,191,192–198] Currently, many studies focus on the fabrication of 4D printed constructs with shape changing abilities such as bending, twisting, elongating, and corrugating against external stimuli such as temperature, humidity, or light. The feasibility of 4D printing relies on the development of new smart materials, novel printing techniques, and mathematical modelling of deformation mechanisms.

Most-widely studied smart materials for 4D printing are temperature-responsive materials. The deformation mechanism of temperature-responsive materials relies on the shape memory effect.[199] Shape memory polymers (SMPs) are typically used because of their ease of printability and capability of recovering their original shape state under an external stimulus after undergoing deformation. The T_g value of SMPs is typically higher than their operating temperatures. Their shapes can be programmed through subsequent heating ($>T_g$) and cooling ($<T_g$) treatments. When the operating temperature is $<T_g$, they adopt a temporary deformed shape. After the temperature increases to $>T_g$, they return to their original shape.[199] For example, SMP fibres were incorporated into an elastomeric matrix to create a hinge structure.[200–202] The hinge could bend with a maximum deformation angle of $\sim 20^\circ$. The deformation angle depends on the T_g value of the SMPs. Wei *et al.*[203] fabricated 4D active shape-changing structures by direct-writing printing of UV photo cross-linkable poly(lactic acid)-based bioinks (Fig. 6a and b) based on SMPs and shape memory nanocomposites (SMNCs). The printed constructs exhibited superior shape memory behaviour, which allowed 3D–1D–3D, 3D–2D–3D, and 3D–3D–3D configuration transformations. Furthermore, to improve their motion freedom, a six-petal leaf with a bilayer structure of paper laminated with polylactic acid was fabricated by Zhang *et al.*[204] The bilayer leaves

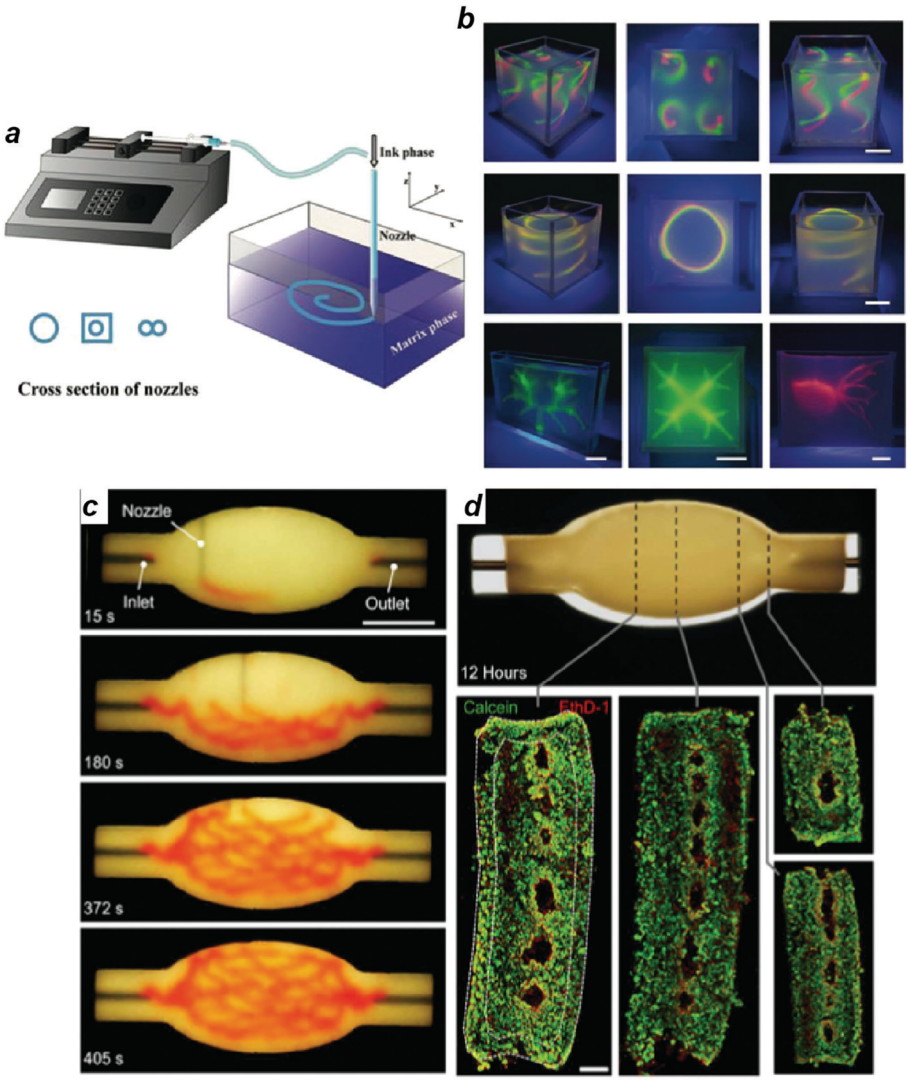

Fig. 5 (a) Schematic illustration of ATPSs. (b) Photographs of double-tornado-shaped, double-spring-shaped, artery-like tree branched network, and goldfish skeleton structures. Reproduced with permission from ref. 188. Copyright 2019, Wiley VCH. (c) An image sequence showing the embedded 3D printing of a branched, hierarchical vascular network within a tissue matrix connected to inlet and outlet tubes. The scale bar is 10 mm. (D) Images of the perfusable tissue construct after 12 h of perfusion (top image) and fluorescence image of live/dead (green/red) cell viability (bottom images). Reproduced with permission from ref. 189. Copyright 2019, AAAS.

uniformly curled into a flower shape upon changing the environment temperature (Fig. 7c–e). This strategy is applicable to creating complex structures with corrugated and helical configurations.

Malachowski *et al.*[205] also reported the fabrication of temperature-responsive multi-fingered grippers. The grippers consist of rigid segments made from poly(propylene fumarate) and stimuli-responsive hinges made from poly(*N*-isopropylacrylamide-*co*-acrylic acid) using the stereolithography technique. The grippers grip drugs at >32 °C and release them into the targeted tissue at body temperature of 37 °C (Fig. 6f–h). Fabrication of containers made from photoresist panels and thermo-responsive PCL hinges was also demonstrated using photolithography (Fig. 6i–l).[206] Similar approaches that used temperature as an external stimulus have been reported by several research groups.[207–209]

Humidity-responsive materials that undergo deformation on taking up or releasing moisture were used for 4D printing.[206,210] Initially, 3D objects printed from inks composed of rigid polymers and humidity-responsive materials were demonstrated by Raviv *et al.*[211] Upon changing the moisture level, the volume of the printed object was extended and folded by 200% from its original state. However, the obtained object was relatively fragile against repeated motion of folding and unfolding. Mao *et al.*[212] printed a structure with anisotropic swelling properties by confining hydrogels in one direction using stiff materials. Gladman *et al.*[213] demonstrated a 4D printed structure with a four times higher transverse swelling strain characteristic than that of longitudinal strain using a hydrogel ink which includes cellulose fibrils. The cellulose fibrils in the hydrogel ink were aligned by the shear forces

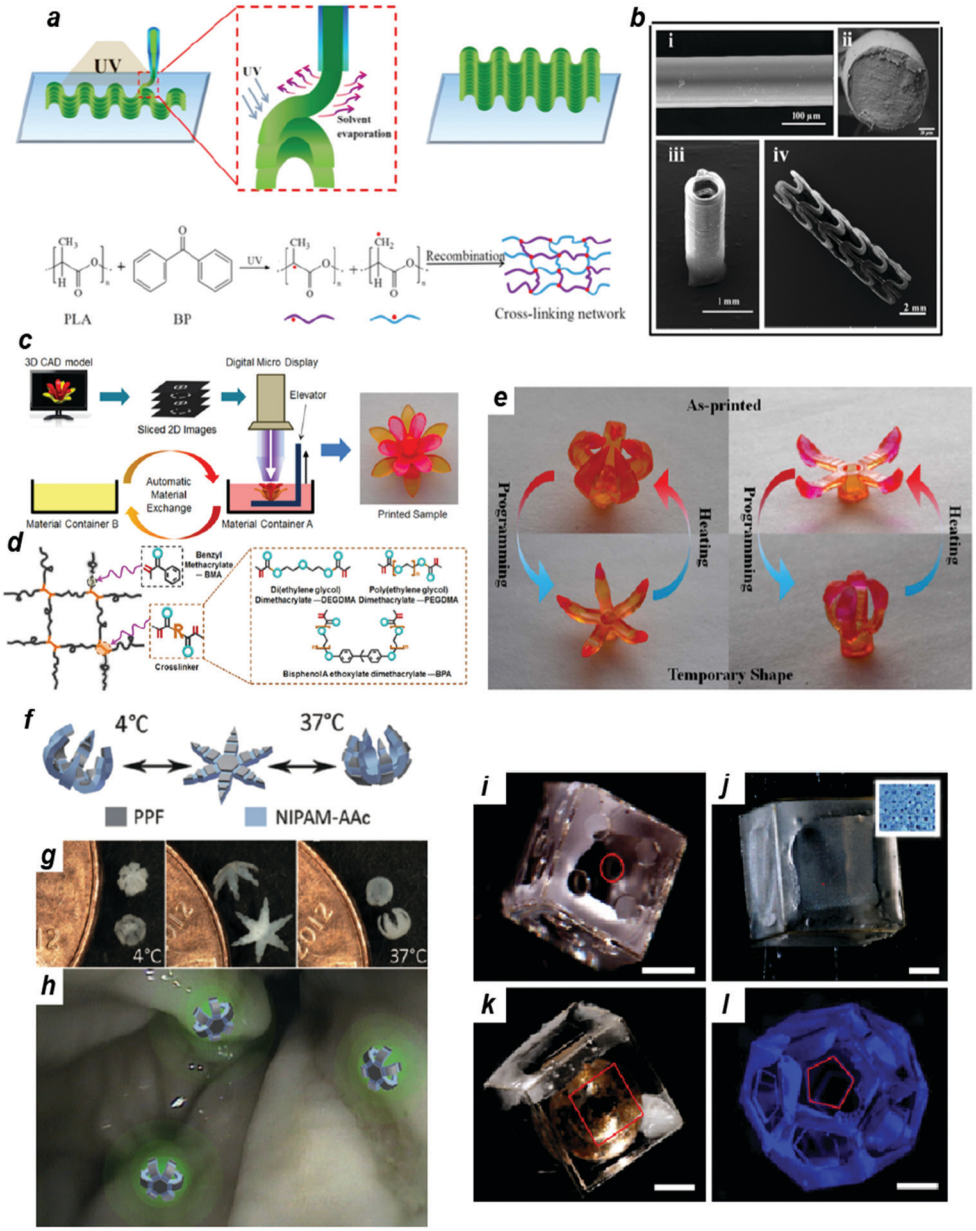

Fig. 6 (a) Schematic illustration of the direct-writing printing of a 4D active shape-changing architecture and the chemical structures of inks. (b) SEM images and 4D active shape-changing behavior of structures printed with c-PLA ink. Reproduced with permission from ref. 203. Copyright 2017, American Chemical Society. (c and d) Schematics of a multimaterial additive manufacturing system. (e) The demonstration of the transition between the as printed shape and temporary shape of multimaterial grippers. Reproduced with permission from ref. 204. Copyright 2016, Nature Publishing Group. (f–h) Design and proof of principle of drug-eluting theragrippers. Reproduced with permission from ref. 205. Copyright 2014, Wiley VCH. (i–l) Photographs of self-folding of multiple containers and versatility in polyhedral shape, size and precise porosity. Reproduced with permission from ref. 206. Copyright 2011, Springer.

generated from the contact between the ink and the print bed. Mulakkal *et al.*[214] also fabricated humidity-responsive natural hydrogel constructs using carboxymethyl cellulose hydrocolloids. Zhang *et al.*[215] designed a hydrogel construct with quick response properties by using hydrophobic thin films derived from cellulose stearoyl esters (CSEs). Their actuation properties could control the changes in the temperature of the surrounding aqueous environment. Other research groups have also developed soft actuators, humidity-responsive sensors, and drug delivery systems by using humidity-responsive hydrogels (*e.g.*, PEGDA) and biodegradable elastomers (*e.g.*, poly(glycerol sebacate)).[216–219]

The use of light-responsive materials offers a basis to develop novel stimuli-responsive constructs and printing techniques because light as a stimulus has the ability to focus energy only on the desired area, enabling rapid and local control or switching of light-responsive materials. The photo-responsive material is locally heated by the absorbed light.

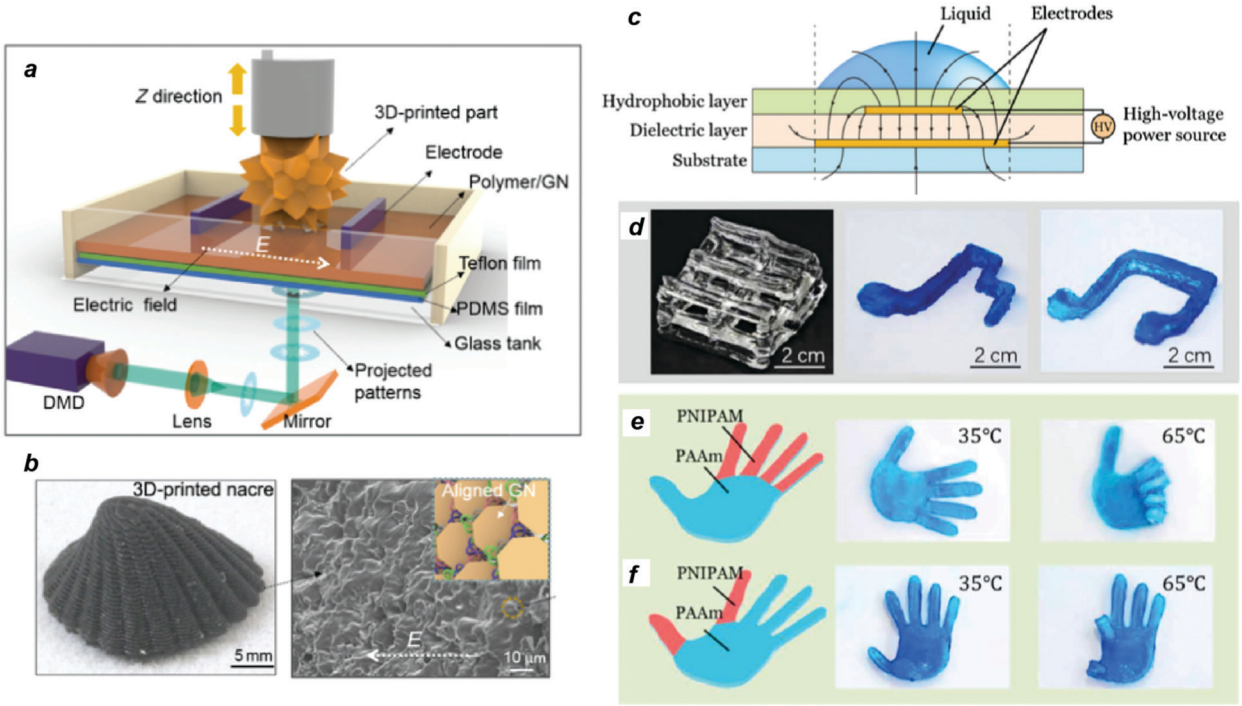

Fig. 7 (a) Schematic diagram of the electrically assisted 3D-printing platform for the construction of nacre-inspired structures, (b) 3D printed nacre with GNs and SEM images showing the surface and cross-section morphology. Reproduced with permission from ref. 230. Copyright 2019, AAAS. (c) Principle of PLEEC. (d) Scaffold-structured hydrogel lattice. (e and f) Polymerized acrylamide (PAAm) and polymerized *N*-isopropyl acrylamide (PNIPAM) hydrogel composites. Reproduced with permission from ref. 232. Copyright 2019, AAAS.

Yang *et al.*[220] demonstrated light-responsive sunflower-like 3D objects composed of carbon black and a PU-based SMP with sequential bud-to-bloom deformation driven by heat generated from the absorbed light. In this mechanism, light was utilized for the deformation of various self-folding structures.[221–223] Wu *et al.*[224] demonstrated the versatility of light sources as external stimuli for patterning bent 4D printed constructs. A drug delivery system has also been developed using a poly(lactic-*co*-glycolic) acid capsule loaded with plasmonic gold nanorods.[225] In this system, the capsule is ruptured by laser irradiation at the resonance wavelength of the gold nanorods.

Electric and magnetic fields can also be used in 4D printing as heat sources. A soft artificial muscle made from a mixture of silicone elastomer and ethanol was reported by Miriyev *et al.*[226] They used a phase shift characteristic from the liquid state to the gas state in ethanol under an applied current to control the volume of the silicon elastomer matrix. Okuzaki *et al.*[227] used polypyrrole (PPy) films to create an origami microrobot, which can be controlled by changing the water absorption or the desorption state through an on/off current. Incorporation of magnetic nanoparticles into a hydrogel-based microgripper successfully allowed them to control the microrobot remotely by applying magnetic fields.[216] Kim *et al.*[228] demonstrated the fabrication of silicon rubber–neodymium–iron–boron (NdFeB) hybrid 3D structures with programmed ferromagnetic domains by applying a magnetic field during printing. They also showed a shape change by magnetic actuation. Apart from physical stimuli such as temperature and light, chemical stimuli (pH and ionic concentration) and biological stimuli (glucose and enzymes) have also attracted much interest for the advancement of 4D printing and related materials and opened a path for constructing new biomedical devices.[229]

As described above, 4D printed constructs have the capability of changing their shape and functionality with time. This time-dependent shape-change ability can provide tremendous potential applications for use in biomedical actuators such as self-bending/tightening valves, staples and stents, biomedical microrobots to deliver and release drugs upon external stimulation for targeted therapy, and biosensors for medical diagnostics. Another intriguing application is the fabrication of scaffolds for tissue regeneration, which allows the scaffolds to mimic the complexity of human tissues that possess a dynamic change in their tissue conformations during the tissue regeneration process. 4D printed tissue constructs with a response to fluctuations in the external environment and geometry change can offer a favourable dynamic microenvironment for tissue regeneration that could not be precisely mimicked in conventional 3D printed tissue constructs.

4.5 Electrically controlled 3D printing

Yang *et al.* made progress in creating 3D hierarchical architectures which mimicked a natural nacre by developing a novel electrically assisted 3D printing technique.[230,231] Their method enabled the fabrication of complex 3D constructs with superior mechanical and electrical properties. They used 3-aminopropyltriethoxysilane grafted graphene nanoplates (GNs) whose

thickness is ~8 nm, diameter is ~25 μm, and surface area is as large as ~120 to 150 m^2 g^{-1} to strengthen the interface with the polymer matrix (epoxy diacrylate and glycol diacrylate). The concept of their 3D printing system with electrical assistance is shown in Fig. 7a. An electric field of 433 V cm^{-1} was applied to align GNs in the polymer matrix during the printing process. GNs in a dielectric polymer ink are polarized under the electric field and gain a higher dipole moment in the direction parallel to the GNs because of the shape anisotropy in the GN, resulting in the alignment of the GNs (Fig. 7b). Their superior mechanical toughness of 1.59 MPa $m^{1/2}$ originates from the synergistic effects of the hydrogen bonding and π–π interactions between the GNs and the polymer and the covalent Si–O–Si bonding between the aminopropyltriethoxysilane grafts on the GNs. This technique is promising for designing and creating a lightweight and strong smart object for use in not only biomedical applications but also transportation, aerospace, and military applications.

Wang *et al.* also proposed a novel method for patterning liquid hydrogels with a resolution as low as 100 μm by introducing a capacitor edge effect, called PLEEC. The PLEEC system consists of five layers (Fig. 7c–f): a pair of silver adhesive electrodes isolated by a dielectric polyimide film layer, an insulating bottom acrylate film layer, and a top Teflon film layer that acts as an insulator to keep the liquidous hydrogels on the top surface isolated from the upper electrode.[232] The top layer should be hydrophobic to send any liquid hydrogels away when the electric field is off. Upon applying the electric field, an electrostatic force is generated to trap the liquidous hydrogels on the top of the surface layer by the capacitor edge effect.

Printed hydrogel objects could effectively respond to the environment temperature. They also demonstrated the fabrication and the operation of ionic high-integrity hydrogel display devices. Current 3D printing techniques using hydrogels as inks largely rely on the physical and chemical properties of hydrogels, which place some constraints on their formability. However, the PLEEC system combined the 3D patterning and stacking processes of hydrogels to offer great opportunities in rapid fabrication of prototype hydrogel constructs with complex geometries and devices with multiple components.

5. Conclusions

3D printing techniques have been receiving growing attention for use in medical applications because of their robust capabilities to produce biomimetic biological structures with ease. This review summarized the conventional and recent advances in 3D printing techniques and materials in biomedical applications. Current technological challenges for 3D printing technologies exist for strategies to achieve higher resolution, higher printing speed, and larger scale while retaining good biocompatibility. Conventional 3D printing techniques have already demonstrated success in generating biological constructs such as cartilage, bone, heart, brain, and muscle, but achieving complex, reproducible, large biological constructs with vascularized architectures suitable for biomedical applications has proved to be challenging. Recent light-assistance based 3D printing techniques, such as computed axial lithography (CAL), show promising potential for achieving a microscale resolution and a speed up to ~1 mm s^{-1}. The combination of such projection stereolithography and dye-added photopolymerizable hydrogels also enabled the fabrication of a lung-mimicking air sac with airways that enable the delivery of oxygen molecules into surrounding blood vessels. Constructs containing liver cells are successfully implanted into mice. The recently developed integrated tissue-organ printer (ITOP) technique also has potential to produce large-scale biological tissue constructs with a complex geometry, human-scale, and high structural integrity. ITOP was found to be feasible to create sizable biological constructs that mimicked the structure of native living tissues: human ear-shaped tissue constructs integrated with cartilage tissues, vascularized functional constructs, and skeletal muscle constructs. Embedded 3D printing techniques also have the potential to obtain complex tissue-like constructs. There remain some challenges, but these technologies greatly advance the field of tissue engineering.

Development of novel biomaterials merged with the desired mechanical properties and high cytocompatibilities, which can recapitulate the extracellular environment, is urgent for 3D printing in biomedical applications. There are still great limitations on the variety of biomaterials that can be applicable for conventional 3D printing in biomedical applications. Because of the prerequisite parameters of biomaterials to possess the specific features of biocompatibility and formability, hydrogels are commonly used as biomaterials for obtaining biological 3D constructs. Therefore, towards the fabrication of complex 3D functional tissues or organs using 3D printing techniques, efforts have been made to develop multi-functional biomaterials and bioinks that can mimic the natural ECM. For mimicking a natural ECM, application of decellularized ECM in 3D printing of biological constructs using extrusion-based and light-assisted methods has been studied. The dECM-based bioinks have heterogeneous constituents such as cell-binding proteins and growth factors present in the ECM of native tissue compared to natural hydrogels, which are highly purified forms of a single ECM component, which enabled researchers to create patient- and organ-specific cell-laden constructs that possess native ECM-like microenvironments. This strategy is useful for developing 3D printed biological tissues and organs because dECM has the potential to modulate biological activities such as cell proliferation, differentiation, migration, and maturation. However, there are still problems with the printing shape fidelity and ethics for its widespread use in 3D printing. Recently developed, multi-functional biomaterials such as stimuli-responsive hydrogels and reversible cross-linking polymers for 4D printing are also promising for creating programmed 3D constructs with complex geometries for biomedical applications and new design systems. The future of biomaterials and biomaterial-based 3D/4D printing is bright. Further improvements in biomaterials and printing technologies will promise the fabrication and engineering of tailor-made functional 3D biological constructs with more complex geometries and artificial organs.

Conflicts of interest

There are no conflicts to declare.

Acknowledgements

This paper was funded by the National Institutes of Health (R01AR074234, R21EB026824, and R01AR073822-01), the Gillian Reny Stepping Strong Center for Trauma Innovation, and AHA Innovative Project Award (19IPLOI34660079).

References

1 C. W. Hull, *US Pat.*, 4575330A, 1989.
2 T. B. Heller, WO1991012120A1, 1990.
3 J. Choi, O. C. Kwon, W. Jo, H. J. Lee and M.-W. Moon, *3D Print. Addit. Manuf.*, 2015, **2**, 159–167.
4 G. P. Dinda, A. K. Dasgupta and J. Mazumder, *Scr. Mater.*, 2012, **67**, 503–506.
5 J. Yeo, G. S. Jung, F. J. Martin-Martinez, S. Ling, G. X. Gu, Z. Qin and M. J. Buehler, *Phys. Scr.*, 2018, **93**, 053003.
6 W. Gao, Y. Zhang, D. Ramanujan, K. Ramani, Y. Chen, C. B. Williams, C. C. L. Wang, Y. C. Shin, S. Zhang and P. D. Zavattieri, *Comput.-Aided Des.*, 2015, **69**, 65–89.
7 J. Edgar and S. Tint, *Johnson Matthey Technol. Rev.*, 2015, **59**, 193–198.
8 G. X. Gu and M. J. Buehler, *Acta Mech.*, 2018, **229**, 4033–4044.
9 F. Libonati, G. X. Gu, Z. Qin, L. Vergani and M. J. Buehler, *Adv. Eng. Mater.*, 2016, **18**, 1354–1363.
10 F. P. W. Melchels, M. A. N. Domingos, T. J. Klein, J. Malda, P. J. Bartolo and D. W. Hutmacher, *Prog. Polym. Sci.*, 2012, **37**, 1079–1104.
11 B. K. Gu, D. J. Choi, S. J. Park, M. S. Kim, C. M. Kang and C. H. Kim, *Biomater. Res.*, 2016, **20**, 12.
12 B. G. Compton and J. A. Lewis, *Adv. Mater.*, 2014, **26**, 5930–5935.
13 U. G. Wegst, H. Bai, E. Saiz, A. P. Tomsia and R. O. Ritchie, *Nat. Mater.*, 2015, **14**, 23–36.
14 S. C. Ligon, R. Liska, J. Stampfl, M. Gurr and R. Mulhaupt, *Chem. Rev.*, 2017, **117**, 10212–10290.
15 G. X. Gu, M. Takaffoli and M. J. Buehler, *Adv. Mater.*, 2017, **29**, 1700060.
16 J. Norman, R. D. Madurawe, C. M. Moore, M. A. Khan and A. Khairuzzaman, *Adv. Drug Delivery Rev.*, 2017, **108**, 39–50.
17 M. Wehner, R. L. Truby, D. J. Fitzgerald, B. Mosadegh, G. M. Whitesides, J. A. Lewis and R. J. Wood, *Nature*, 2016, **536**, 451–455.
18 T. N. Sullivan, A. Pissarenko, S. A. Herrera, D. Kisailus, V. A. Lubarda and M. A. Meyers, *Acta Biomater.*, 2016, **41**, 27–39.
19 S. G. Uzel, R. J. Platt, V. Subramanian, T. M. Pearl, C. J. Rowlands, V. Chan, L. A. Boyer, P. T. So and R. D. Kamm, *Sci. Adv.*, 2016, **2**, e1501429.
20 B. Zhang, L. Gao, L. Ma, Y. Luo, H. Yang and Z. Cui, *Engineering*, 2019, **5**, 777–794.
21 A. T. Gaynor, N. A. Meisel, C. B. Williams and J. K. Guest, *J. Manuf. Sci. Eng.*, 2014, **136**, 061015.
22 T. Zegard and G. H. Paulino, *Struct. Multidiscip. Optim.*, 2015, **53**, 175–192.
23 G. X. Gu, M. Takaffoli, A. J. Hsieh and M. J. Buehler, *Extreme Mech. Lett.*, 2016, **9**, 317–323.
24 G. X. Gu, C.-T. Chen, D. J. Richmond and M. J. Buehler, *Mater. Horiz.*, 2018, **5**, 939–945.
25 G. X. Gu, S. Wettermark and M. J. Buehler, *Addit. Manuf.*, 2017, **17**, 47–54.
26 B. H. Jared, M. A. Aguilo, L. L. Beghini, B. L. Boyce, B. W. Clark, A. Cook, B. J. Kaehr and J. Robbins, *Scr. Mater.*, 2017, **135**, 141–147.
27 A. J. Capel, R. P. Rimington, M. P. Lewis and S. D. R. Christie, Nature Reviews, *Chemistry*, 2018, **2**, 422–436.
28 N. A. Peppas, J. Z. Hilt, A. Khademhosseini and R. Langer, *Adv. Mater.*, 2006, **18**, 1345–1360.
29 B. Holmes, W. Zhu, J. Li, J. D. Lee and L. G. Zhang, *Tissue Eng., Part A*, 2015, **21**, 403–415.
30 C. R. Deckard, *US Pat.*, 4863538, 1986.
31 H. H. Hamzah, S. A. Shafiee, A. Abdalla and B. A. Patel, *Electrochem. Commun.*, 2018, **96**, 27–31.
32 C. E. Blohm, ReferencePoint Press, 2018.
33 F. Dolati, Y. Yu, Y. Zhang, A. M. De Jesus, E. A. Sander and I. T. Ozbolat, *Nanotechnology*, 2014, **25**, 145101.
34 Y. J. Choi, T. G. Kim, J. Jeong, H. G. Yi, J. W. Park, W. Hwang and D. W. Cho, *Adv. Healthcare Mater.*, 2016, **5**, 2636–2645.
35 N. Cubo, M. Garcia, J. F. Del Canizo, D. Velasco and J. L. Jorcano, *Biofabrication*, 2016, **9**, 015006.
36 H. W. Kang, S. J. Lee, I. K. Ko, C. Kengla, J. J. Yoo and A. Atala, *Nat. Biotechnol.*, 2016, **34**, 312–319.
37 Y. Morimoto, H. Onoe and S. Takeuchi, *Sci. Robot.*, 2018, **3**, eaat4440.
38 D. B. Kolesky, K. A. Homan, M. A. Skylar-Scott and J. A. Lewis, *Proc. Natl. Acad. Sci. U. S. A.*, 2016, **113**, 3179–3184.
39 C. Norotte, F. S. Marga, L. E. Niklason and G. Forgacs, *Biomaterials*, 2009, **30**, 5910–5917.
40 W. Zhu, X. Qu, J. Zhu, X. Ma, S. Patel, J. Liu, P. Wang, C. S. Lai, M. Gou, Y. Xu, K. Zhang and S. Chen, *Biomaterials*, 2017, **124**, 106–115.
41 N. S. Bhise, V. Manoharan, S. Massa, A. Tamayol, M. Ghaderi, M. Miscuglio, Q. Lang, Y. Shrike Zhang, S. R. Shin, G. Calzone, N. Annabi, T. D. Shupe, C. E. Bishop, A. Atala, M. R. Dokmeci and A. Khademhosseini, *Biofabrication*, 2016, **8**, 014101.
42 F. Fu, Z. Chen, Z. Zhao, H. Wang, L. Shang, Z. Gu and Y. Zhao, *Proc. Natl. Acad. Sci. U. S. A.*, 2017, **114**, 5900–5905.
43 H. Lee and D. W. Cho, *Lab Chip*, 2016, **16**, 2618–2625.
44 J. U. Lind, T. A. Busbee, A. D. Valentine, F. S. Pasqualini, H. Yuan, M. Yadid, S. J. Park, A. Kotikian, A. P. Nesmith, P. H. Campbell, J. J. Vlassak, J. A. Lewis and K. K. Parker, *Nat. Mater.*, 2017, **16**, 303–308.
45 S. Bertlein, G. Brown, K. S. Lim, T. Jungst, T. Boeck, T. Blunk, J. Tessmar, G. J. Hooper, T. B. F. Woodfield and J. Groll, *Adv. Mater.*, 2017, **29**, 1703404.

46 W. Liu, Y. S. Zhang, M. A. Heinrich, F. De Ferrari, H. L. Jang, S. M. Bakht, M. M. Alvarez, J. Yang, Y. C. Li, G. Trujillo-de Santiago, A. K. Miri, K. Zhu, P. Khoshakhlagh, G. Prakash, H. Cheng, X. Guan, Z. Zhong, J. Ju, G. H. Zhu, X. Jin, S. R. Shin, M. R. Dokmeci and A. Khademhosseini, *Adv. Mater.*, 2017, **29**, 1604630.
47 C. Xu, W. Lee, G. Dai and Y. Hong, *ACS Appl. Mater. Interfaces*, 2018, **10**, 9969–9979.
48 W. Liu, M. A. Heinrich, Y. Zhou, A. Akpek, N. Hu, X. Liu, X. Guan, Z. Zhong, X. Jin, A. Khademhosseini and Y. S. Zhang, *Adv. Healthcare Mater.*, 2017, **6**, 1601451.
49 P. Apelgren, M. Amoroso, A. Lindahl, C. Brantsing, N. Rotter, P. Gatenholm and L. Kolby, *PLoS One*, 2017, **12**, e0189428.
50 Z. Wu, X. Su, Y. Xu, B. Kong, W. Sun and S. Mi, *Sci. Rep.*, 2016, **6**, 24474.
51 B. Byambaa, N. Annabi, K. Yue, G. Trujillo-de Santiago, M. M. Alvarez, W. Jia, M. Kazemzadeh-Narbat, S. R. Shin, A. Tamayol and A. Khademhosseini, *Adv. Healthcare Mater.*, 2017, **6**, 1700015.
52 J. Yin, M. Yan, Y. Wang, J. Fu and H. Suo, *ACS Appl. Mater. Interfaces*, 2018, **10**, 6849–6857.
53 Q. Gu, E. Tomaskovic-Crook, G. G. Wallace and J. M. Crook, *Adv. Healthcare Mater.*, 2017, **6**, 1700175.
54 Z. Wang, X. Jin, Z. Tian, F. Menard, J. F. Holzman and K. Kim, *Adv. Healthcare Mater.*, 2018, **7**, e1701249.
55 N. D. Dinh, R. Luo, M. T. A. Christine, W. N. Lin, W. C. Shih, J. C. Goh and C. H. Chen, *Small*, 2017, **13**, 1700684.
56 V. Keriquel, H. Oliveira, M. Remy, S. Ziane, S. Delmond, B. Rousseau, S. Rey, S. Catros, J. Amedee, F. Guillemot and J. C. Fricain, *Sci. Rep.*, 2017, **7**, 1778.
57 Z. Zhang, R. Xiong, R. Mei, Y. Huang and D. B. Chrisey, *Langmuir*, 2015, **31**, 6447–6456.
58 S. Sakai, H. Kamei, T. Mori, T. Hotta, H. Ohi, M. Nakahata and M. Taya, *Biomacromolecules*, 2018, **19**, 672–679.
59 G. Gao, A. F. Schilling, K. Hubbell, T. Yonezawa, D. Truong, Y. Hong, G. Dai and X. Cui, *Biotechnol. Lett.*, 2015, **37**, 2349–2355.
60 M. Khanmohammadi, M. B. Dastjerdi, A. Ai, A. Ahmadi, A. Godarzi, A. Rahimi and J. Ai, *Biomater. Sci.*, 2018, **6**, 1286–1298.
61 K. Christensen, C. Xu, W. Chai, Z. Zhang, J. Fu and Y. Huang, *Biotechnol. Bioeng.*, 2015, **112**, 1047–1055.
62 L. R. Hart, S. Li, C. Sturgess, R. Wildman, J. R. Jones and W. Hayes, *ACS Appl. Mater. Interfaces*, 2016, **8**, 3115–3122.
63 A. A. S. Samson, J. Lee and J. M. Song, *Sci. Rep.*, 2018, **8**, 591.
64 C. C. W. Tse and P. J. Smith, *Methods Mol. Biol.*, 2018, **1771**, 107–117.
65 J. Hendriks, C. Willem Visser, S. Henke, J. Leijten, D. B. Saris, C. Sun, D. Lohse and M. Karperien, *Sci. Rep.*, 2015, **5**, 11304.
66 X. Ma, J. Liu, W. Zhu, M. Tang, N. Lawrence, C. Yu, M. Gou and S. Chen, *Adv. Drug Delivery Rev.*, 2018, **132**, 235–251.
67 H. Gudapati, M. Dey and I. Ozbolat, *Biomaterials*, 2016, **102**, 20–42.
68 K. Holzl, S. Lin, L. Tytgat, S. Van Vlierberghe, L. Gu and A. Ovsianikov, *Biofabrication*, 2016, **8**, 032002.
69 I. T. Ozbolat and Y. Yu, *IEEE Trans. Biomed. Eng.*, 2013, **60**, 691–699.
70 I. T. Ozbolat, K. K. Moncal and H. Gudapati, *Addit. Manuf.*, 2017, **13**, 179–200.
71 W. Jia, P. S. Gungor-Ozkerim, Y. S. Zhang, K. Yue, K. Zhu, W. Liu, Q. Pi, B. Byambaa, M. R. Dokmeci, S. R. Shin and A. Khademhosseini, *Biomaterials*, 2016, **106**, 58–68.
72 A. D. Graham, S. N. Olof, M. J. Burke, J. P. K. Armstrong, E. A. Mikhailova, J. G. Nicholson, S. J. Box, F. G. Szele, A. W. Perriman and H. Bayley, *Sci. Rep.*, 2017, **7**, 7004.
73 I. T. Ozbolat and M. Hospodiuk, *Biomaterials*, 2016, **76**, 321–343.
74 E. Axpe and M. L. Oyen, *Int. J. Mol. Sci.*, 2016, **17**, 1976.
75 R. Langer and J. P. Vacanti, *Science*, 1993, **260**, 920–926.
76 F. R. de Gruijl, H. J. van Kranen and L. H. F. Mullenders, *J. Photochem. Photobiol., B*, 2001, **63**, 19–27.
77 F. Momeni, S. M. Mehdi, N. Hassani, X. Liu and J. Ni, *Mater. Des.*, 2017, **122**, 42–79.
78 T. K. Merceron, M. Burt, Y. J. Seol, H. W. Kang, S. J. Lee, J. J. Yoo and A. Atala, *Biofabrication*, 2015, **7**, 035003.
79 F. Y. Hsieh, H. H. Lin and S. H. Hsu, *Biomaterials*, 2015, **71**, 48–57.
80 Y. Huang, K. He and X. Wang, *Mater. Sci. Eng., C*, 2013, **33**, 3220–3229.
81 K. C. Hung, C. S. Tseng, L. G. Dai and S. H. Hsu, *Biomaterials*, 2016, **83**, 156–168.
82 T. Xu, W. Zhao, J. M. Zhu, M. Z. Albanna, J. J. Yoo and A. Atala, *Biomaterials*, 2013, **34**, 130–139.
83 C. Xu, W. Chai, Y. Huang and R. R. Markwald, *Biotechnol. Bioeng.*, 2012, **109**, 3152–3160.
84 I. T. Ozbolat, H. Chen and Y. Yu, *Robot. Comput. Integr. Manuf.*, 2014, **30**, 295–304.
85 S. Ahn, H. Lee and G. Kim, *Carbohydr. Polym.*, 2013, **98**, 936–942.
86 H. Lee, S. Ahn, L. J. Bonassar, W. Chun and G. Kim, *Tissue Eng., Part C*, 2013, **19**, 784–793.
87 M. T. Poldervaart, B. Goversen, M. de Ruijter, A. Abbadessa, F. P. W. Melchels, F. C. Oner, W. J. A. Dhert, T. Vermonden and J. Alblas, *PLoS One*, 2017, **12**, e0177628.
88 J.-H. Shim, J.-S. Lee, J. Y. Kim and D.-W. Cho, *J. Micromech. Microeng.*, 2012, **22**, 085014.
89 B. Guillotin, A. Souquet, S. Catros, M. Duocastella, B. Pippenger, S. Bellance, R. Bareille, M. Remy, L. Bordenave, J. Amedee and F. Guillemot, *Biomaterials*, 2010, **31**, 7250–7256.
90 A. D. Pallab Datta, Y. Yu, D. Hayes, H. Gudapati and I. T. Ozbolat, *Int. J. Bioprint.*, 2017, **3**, 109–120.
91 F. You, B. F. Eames and X. Chen, *Int. J. Mol. Sci.*, 2017, **18**, 1597.
92 J. E. Snyder, Q. Hamid, C. Wang, R. Chang, K. Emami, H. Wu and W. Sun, *Biofabrication*, 2011, **3**, 034112.
93 S. Rhee, J. L. Puetzer, B. N. Mason, C. A. Reinhart-King and L. J. Bonassar, *ACS Biomater. Sci. Eng.*, 2016, **2**, 1800–1805.
94 W. Lee, V. K. Lee, S. Polio, K. Fischer, J.-H. Lee, J.-K. Park and S.-S. Yoo, TRANSDUCERS 2009-2009 International

Solid-State Sensors, Actuators and Microsystems Conference, 2009, 10916916, DOI: 10.1109/SENSOR.2009.5285591.
95 S. Michael, H. Sorg, C. T. Peck, L. Koch, A. Deiwick, B. Chichkov, P. M. Vogt and K. Reimers, *PLoS One*, 2013, **8**, e57741.
96 X. Wang, Y. Yan, Y. Pan, Z. Xiong, H. Liu, J. Cheng, F. Liu, F. Lin, R. Wu, R. Zhang and Q. Lu, *Tissue Eng.*, 2006, **12**, 83–90.
97 N. R. Schiele, D. B. Chrisey and D. T. Corr, *Tissue Eng., Part C*, 2011, **17**, 289–298.
98 J. Visser, B. Peters, T. J. Burger, J. Boomstra, W. J. Dhert, F. P. Melchels and J. Malda, *Biofabrication*, 2013, **5**, 035007.
99 A. Skardal, J. Zhang and G. D. Prestwich, *Biomaterials*, 2010, **31**, 6173–6181.
100 W. L. Ng, W. Y. Yeong and M. W. Naing, *Procedia CIRP*, 2016, **49**, 105–112.
101 P. B. Malafaya and R. L. Reis, *Acta Biomater.*, 2009, **5**, 644–660.
102 L. E. Bertassoni, M. Cecconi, V. Manoharan, M. Nikkhah, J. Hjortnaes, A. L. Cristino, G. Barabaschi, D. Demarchi, M. R. Dokmeci, Y. Yang and A. Khademhosseini, *Lab Chip*, 2014, **14**, 2202–2211.
103 X. Ma, X. Qu, W. Zhu, Y. S. Li, S. Yuan, H. Zhang, J. Liu, P. Wang, C. S. Lai, F. Zanella, G. S. Feng, F. Sheikh, S. Chien and S. Chen, *Proc. Natl. Acad. Sci. U. S. A.*, 2016, **113**, 2206–2211.
104 P. Soman, P. H. Chung, A. P. Zhang and S. Chen, *Biotechnol. Bioeng.*, 2013, **110**, 3038–3047.
105 J. S. Lee, J. M. Hong, J. W. Jung, J. H. Shim, J. H. Oh and D. W. Cho, *Biofabrication*, 2014, **6**, 024103.
106 Z. Zhang, Y. Jin, J. Yin, C. Xu, R. Xiong, K. Christensen, B. R. Ringeisen, D. B. Chrisey and Y. Huang, *Appl. Phys. Rev.*, 2018, **5**, 041304.
107 M. Chaouat, C. Le Visage, W. E. Baille, B. Escoubet, F. Chaubet, M. A. Mateescu and D. A. Letourneur, *Adv. Funct. Mater.*, 2008, **18**, 2855–2861.
108 V. Chan, P. Zorlutuna, J. H. Jeong, H. Kong and R. Bashir, *Lab Chip*, 2010, **10**, 2062–2070.
109 D. B. Kolesky, R. L. Truby, A. S. Gladman, T. A. Busbee, K. A. Homan and J. A. Lewis, *Adv. Mater.*, 2014, **26**, 3124–3130.
110 Z. Wang, R. Abdulla, B. Parker, R. Samanipour, S. Ghosh and K. Kim, *Biofabrication*, 2015, **7**, 045009.
111 C. B. Hutson, J. W. Nichol, H. Aubin, H. Bae, S. Yamanlar, S. Al-Haque, S. T. Koshy and A. Khademhosseini, *Tissue Eng., Part A*, 2011, **17**, 1713–1723.
112 T. Miao, E. J. Miller, C. McKenzie and R. A. Oldinski, *J. Mater. Chem. B*, 2015, **3**, 9242–9249.
113 J. E. Kim, S. H. Kim and Y. Jung, *Tissue Eng. Regener. Med.*, 2016, **13**, 636–646.
114 J. Jang, J. Y. Park, G. Gao and D. W. Cho, *Biomaterials*, 2018, **156**, 88–106.
115 M. Muller, J. Becher, M. Schnabelrauch and M. Zenobi-Wong, *Biofabrication*, 2015, **7**, 035006.
116 J. P. Armstrong, M. Burke, B. M. Carter, S. A. Davis and A. W. Perriman, *Adv. Healthcare Mater.*, 2016, **5**, 1724–1730.
117 W. Schuurman, V. Khristov, M. W. Pot, P. R. van Weeren, W. J. Dhert and J. Malda, *Biofabrication*, 2011, **3**, 021001.
118 J. H. Shim, J. Y. Kim, M. Park, J. Park and D. W. Cho, *Biofabrication*, 2011, **3**, 034102.
119 T. Xu, K. W. Binder, M. Z. Albanna, D. Dice, W. Zhao, J. J. Yoo and A. Atala, *Biofabrication*, 2013, **5**, 015001.
120 B. P. Hung, B. A. Naved, E. L. Nyberg, M. Dias, C. A. Holmes, J. H. Elisseeff, A. H. Dorafshar and W. L. Grayson, *ACS Biomater. Sci. Eng.*, 2016, **2**, 1806–1816.
121 Y. Yu, K. K. Moncal, J. Li, W. Peng, I. Rivero, J. A. Martin and I. T. Ozbolat, *Sci. Rep.*, 2016, **6**, 28714.
122 B. Duan, *Ann. Biomed. Eng.*, 2017, **45**, 195–209.
123 C. M. Owens, F. Marga, G. Forgacs and C. M. Heesch, *Biofabrication*, 2013, **5**, 045007.
124 K. C. Hribar, P. Soman, J. Warner, P. Chung and S. Chen, *Lab Chip*, 2014, **14**, 268–275.
125 Y. Lu, G. Mapili, G. Suhali, S. Chen and K. Roy, *J. Biomed. Mater. Res., Part A*, 2006, **77**, 396–405.
126 W. Zhang, L.-H. Han and S. Chen, *J. Manuf. Sci. Eng.*, 2010, **132**, 030907.
127 A. P. Zhang, X. Qu, P. Soman, K. C. Hribar, J. W. Lee, S. Chen and S. He, *Adv. Mater.*, 2012, **24**, 4266–4270.
128 J. R. Tumbleston, D. Shirvanyants, N. Ermoshkin, R. Janusziewicz, A. R. Johnson, D. Kelly, K. Chen, R. Pinschmidt, J. P. Rolland, A. Ermoshkin, E. T. Samulski and J. M. DeSimone, *Science*, 2015, **347**, 1349–1352.
129 K. C. Hribar, D. Finlay, X. Ma, X. Qu, M. G. Ondeck, P. H. Chung, F. Zanella, A. J. Engler, F. Sheikh, K. Vuori and S. C. Chen, *Lab Chip*, 2015, **15**, 2412–2418.
130 J. Liu, H. H. Hwang, P. Wang, G. Whang and S. Chen, *Lab Chip*, 2016, **16**, 1430–1438.
131 S. P. Grogan, P. H. Chung, P. Soman, P. Chen, M. K. Lotz, S. Chen and D. D. D'Lima, *Acta Biomater.*, 2013, **9**, 7218–7226.
132 K. Arcaute, B. K. Mann and R. B. Wicker, *Stereolithography: Materials, Processes and Applications*, Springer, 2011.
133 J. W. Lee, P. Soman, J. H. Park, S. Chen and D. W. Cho, *PLoS One*, 2016, **11**, e0155681.
134 S. A. Skoog, P. L. Goering and R. J. Narayan, *J. Mater. Sci.: Mater. Med.*, 2014, **25**, 845–856.
135 J. Warner, P. Soman, W. Zhu, M. Tom and S. Chen, *ACS Biomater. Sci. Eng.*, 2016, **2**, 1763–1770.
136 S. H. Park, D. Y. Yang and K. S. Lee, *Laser Photonics Rev.*, 2009, **3**, 1–11.
137 B. Cumpston, S. Ananthavel and S. Barlow, *et al.*, *Nature*, 1999, **398**, 51–54.
138 W. R. Zipfel, R. M. Williams and W. W. Webb, *Nat. Biotechnol.*, 2003, **21**, 1369–1377.
139 M. Farsari and B. N. Chichkov, *Nat. Photonics*, 2009, **3**, 450–452.
140 D. Perevoznik, R. Nazir, R. Kiyan, K. Kurselis, B. Koszarna, D. T. Gryko and B. N. Chichkov, *Opt. Express*, 2019, **27**, 25119–25125.
141 T.-S. Jang, H.-D. Jung, H. M. Pan, W. T. Han, S. Chen and J. Song, *Int. J. Bioprint.*, 2018, **4**, 126.

142 R. G. Wylie, S. Ahsan, Y. Aizawa, K. L. Maxwell, C. M. Morshead and M. S. Shoichet, *Nat. Mater.*, 2011, **10**, 799–806.
143 R. L. Truby and J. A. Lewis, *Nature*, 2016, **540**, 371–378.
144 J. F. Xing, M. L. Zheng and X. M. Duan, *Chem. Soc. Rev.*, 2015, **44**, 5031–5039.
145 A. Bell, M. Kofron and V. Nistor, *Biofabrication*, 2015, **7**, 035007.
146 T. Yucel, P. Cebe and D. L. Kaplan, *Biophys. J.*, 2009, **97**, 2044–2050.
147 C. Colosi, S. R. Shin, V. Manoharan, S. Massa, M. Costantini, A. Barbetta, M. R. Dokmeci, M. Dentini and A. Khademhosseini, *Adv. Mater.*, 2016, **28**, 677–684.
148 N. E. Fedorovich, J. R. De Wijn, A. J. Verbout, J. Alblas and W. J. Dhert, *Tissue Eng., Part A*, 2008, **14**, 127–133.
149 D. F. Duarte Campos, A. Blaeser, A. Korsten, S. Neuss, J. Jakel, M. Vogt and H. Fischer, *Tissue Eng., Part A*, 2015, **21**, 740–756.
150 T. Billiet, E. Gevaert, T. De Schryver, M. Cornelissen and P. Dubruel, *Biomaterials*, 2014, **35**, 49–62.
151 R. Levato, W. R. Webb, I. A. Otto, A. Mensinga, Y. Zhang, M. van Rijen, R. van Weeren, I. M. Khan and J. Malda, *Acta Biomater.*, 2017, **61**, 41–53.
152 V. H. Mouser, F. P. Melchels, J. Visser, W. J. Dhert, D. Gawlitta and J. Malda, *Biofabrication*, 2016, **8**, 035003.
153 G. C. J. Brown, K. S. Lim, B. L. Farrugia, G. J. Hooper and T. B. F. Woodfield, *Macromol. Biosci.*, 2017, **17**, 1700158.
154 R. Levato, J. Visser, J. A. Planell, E. Engel, J. Malda and M. A. Mateos-Timoneda, *Biofabrication*, 2014, **6**, 035020.
155 B. Duan, L. A. Hockaday, K. H. Kang and J. T. Butcher, *J. Biomed. Mater. Res., Part A*, 2013, **101**, 1255–1264.
156 C. R. Pimentel, S. K. Ko, C. Caviglia, A. Wolff, J. Emneus, S. S. Keller and M. Dufva, *Acta Biomater.*, 2018, **65**, 174–184.
157 M. A. Malana, R. Zohra and M. S. Khan, *Korea-Aust. Rheol. J.*, 2012, **24**, 155–162.
158 W. Zhang, P. Soman, K. Meggs, X. Qu and S. Chen, *Adv. Funct. Mater.*, 2013, **23**, 3226–3232.
159 J. Malda, J. Visser, F. P. Melchels, T. Jungst, W. E. Hennink, W. J. Dhert, J. Groll and D. W. Hutmacher, *Adv. Mater.*, 2013, **25**, 5011–5028.
160 B. D. Ratner, A. S. Hoffman, F. J. Schoen and J. E. Lemons, *Biomaterials science: an introduction to materials in medicine*, 2013.
161 L. G. Zhang, J. Fisher and K. Leong, *3D Bioprinting and Nanotechnology in Tissue Engineering and Regenerative Medicine*, Elsevier Academic Press, 2015.
162 H. Martínez Ávila, S. Schwarz, N. Rotter and P. Gatenholm, *Bioprinting*, 2016, **1–2**, 22–35.
163 L. Ouyang, C. B. Highley, C. B. Rodell, W. Sun and J. A. Burdick, *ACS Biomater. Sci. Eng.*, 2016, **2**, 1743–1751.
164 Q. Gao, Y. He, J. Z. Fu, A. Liu and L. Ma, *Biomaterials*, 2015, **61**, 203–215.
165 A. Faulkner-Jones, C. Fyfe, D. J. Cornelissen, J. Gardner, J. King, A. Courtney and W. Shu, *Biofabrication*, 2015, **7**, 044102.
166 T. J. Keane and S. F. Badylak, *Semin. Pediatr. Surg.*, 2014, **23**, 112–118.
167 M. Hospodiuk, M. Dey, D. Sosnoski and I. T. Ozbolat, *Biotechnol. Adv.*, 2017, **35**, 217–239.
168 F. Pati, J. Jang, D. H. Ha, S. Won Kim, J. W. Rhie, J. H. Shim, D. H. Kim and D. W. Cho, *Nat. Commun.*, 2014, **5**, 3935.
169 H. Lee, W. Han, H. Kim, D. H. Ha, J. Jang, B. S. Kim and D. W. Cho, *Biomacromolecules*, 2017, **18**, 1229–1237.
170 J. Gopinathan and I. Noh, *Biomater. Res.*, 2018, **22**, 11.
171 N. Ashammakhi, S. Ahadian, C. Xu, H. Montazerian, H. Ko, R. Nasiri, N. Barros and A. Khademhosseini, *Mater. Today Bio*, 2019, **1**, 100008.
172 A. A. Pawar, G. Saada, I. Cooperstein, L. Larush, J. A. Jackman, S. R. Tabaei, N. J. Cho and S. Magdassi, *Sci. Adv.*, 2016, **2**, e1501381.
173 P. M. Crapo, T. W. Gilbert and S. F. Badylak, *Biomaterials*, 2011, **32**, 3233–3243.
174 T. L. Sellaro, A. Ranade, D. M. Faulk, G. P. McCabe, K. Dorko, S. F. Badylak and S. C. Strom, *Tissue Eng., Part A*, 2010, **16**, 1075–1082.
175 B. Perniconi, A. Costa, P. Aulino, L. Teodori, S. Adamo and D. Coletti, *Biomaterials*, 2011, **32**, 7870–7882.
176 B. E. Kelly, I. Bhattacharya, H. Heidari, M. Shusteff, C. M. Spadaccini and H. K. Taylor, *Science*, 2019, **363**, 1075–1079.
177 G. N. Hounsfield, *US Pat.*, 3778614, 1973.
178 J. Kastner and C. Heinzl, *X-ray Computed Tomography for Non-destructive Testing and Materials Characterization (Integrated Imaging and Vision Techniques for Industrial Inspection)*, Springer, 2015.
179 T. Bortfeld, J. Burkelbach, R. Boesecke and W. Schlegel, *Phys. Med. Biol.*, 1990, **35**, 1423–1434.
180 B. Grigoryan, S. J. Paulsen, D. C. Corbett, D. W. Sazer, C. L. Fortin, A. J. Zaita, P. T. Greenfield, N. J. Calafat, J. P. Gounley, A. H. Ta, F. Johansson, A. Randles, J. E. Rosenkrantz, J. D. Louis-Rosenberg, P. A. Galie, K. R. Stevens and J. S. Miller, *Science*, 2019, **364**, 458–464.
181 M. A. Skylar-Scott, J. Mueller, C. W. Visser and J. A. Lewis, *Nature*, 2019, **575**, 330–335.
182 W. Wu, A. DeConinck and J. A. Lewis, *Adv. Mater.*, 2011, **23**, H178–H183.
183 T. Bhattacharjee, S. M. Zehnder, K. G. Rowe, S. Jain, R. M. Nixon, W. G. Sawyer and T. E. Angelini, *Sci. Adv.*, 2015, **1**, e1500655.
184 T. J. Hinton, Q. Jallerat, R. N. Palchesko, J. H. Park, M. S. Grodzicki, H. J. Shue, M. H. Ramadan, A. R. Hudson and A. W. Feinberg, *Sci. Adv.*, 2015, **1**, e1500758.
185 C. B. Highley, C. B. Rodell and J. A. Burdick, *Adv. Mater.*, 2015, **27**, 5075–5079.
186 C. Loebel, C. B. Rodell, M. H. Chen and J. A. Burdick, *Nat. Protoc.*, 2017, **12**, 1521–1541.
187 C. B. Highley, K. H. Song, A. C. Daly and J. A. Burdick, *Adv. Sci.*, 2019, **6**, 1801076.
188 G. Luo, Y. Yu, Y. Yuan, X. Chen, Z. Liu and T. Kong, *Adv. Mater.*, 2019, **31**, e1904631.
189 M. A. Skylar-Scott, S. G. M. Uzel, L. L. Nam, J. H. Ahrens, R. L. Truby, S. Damaraju and J. A. Lewis, *Sci. Adv.*, 2019, **5**, eaaw2459.

190 S. Tibbits, *Architectural Design*, 2014, **84**, 116–121.
191 Z. X. Khoo, J. E. M. Teoh, Y. Liu, C. K. Chua, S. Yang, J. An, K. F. Leong and W. Y. Yeong, *Virtual Phys. Prototyping*, 2015, **10**, 103–122.
192 Z. Zhang, K. G. Demir and G. X. Gu, *Int. J. Smart Nano Mater.*, 2019, **10**, 205–224.
193 S. Miao, W. Zhu, N. J. Castro, M. Nowicki, X. Zhou, H. Cui, J. P. Fisher and L. G. Zhang, *Sci. Rep.*, 2016, **6**, 27226.
194 M. Bodaghi, A. R. Damanpack and W. H. Liao, *Smart Mater. Struct.*, 2016, **25**, 105034.
195 T.-H. Kwok, C. C. L. Wang, D. Deng, Y. Zhang and Y. Chen, *J. Mech. Design*, 2015, **137**, 111413.
196 Y. Zhang, F. Zhang, Z. Yan, Q. Ma, X. Li, Y. Huang and J. A. Rogers, *Nat. Rev. Mater.*, 2017, **2**, 17019.
197 Q. Ge, A. H. Sakhaei, H. Lee, C. K. Dunn, N. X. Fang and M. L. Dunn, *Sci. Rep.*, 2016, **6**, 31110.
198 K. Yu, A. Ritchie, Y. Mao, M. L. Dunn and H. J. Qi, *Procedia IUTAM*, 2015, **12**, 193–203.
199 F. Momeni, S. Sabzpoushan, R. Valizadeh, M. R. Morad, X. Liu and J. Ni, *Renewable Energy*, 2019, **130**, 329–351.
200 M. D. Hager, S. Bode, C. Weber and U. S. Schubert, *Prog. Polym. Sci.*, 2015, **49-50**, 3–33.
201 Q. Ge, H. J. Qi and M. L. Dunn, *Appl. Phys. Lett.*, 2013, **103**, 131901.
202 X. Lan, Y. Liu, H. Lv, X. Wang, J. Leng and S. Du, *Smart Mater. Struct.*, 2009, **18**, 024002.
203 H. Wei, Q. Zhang, Y. Yao, L. Liu, Y. Liu and J. Leng, *ACS Appl. Mater. Interfaces*, 2017, **9**, 876–883.
204 Q. Zhang, K. Zhang and G. Hu, *Sci. Rep.*, 2016, **6**, 22431.
205 K. Malachowski, J. Breger, H. R. Kwag, M. O. Wang, J. P. Fisher, F. M. Selaru and D. H. Gracias, *Angew. Chem., Int. Ed.*, 2014, **53**, 8045–8049.
206 A. Azam, K. E. Laflin, M. Jamal, R. Fernandes and D. H. Gracias, *Biomed. Microdevices*, 2011, **13**, 51–58.
207 H. Therien-Aubin, Z. L. Wu, Z. Nie and E. Kumacheva, *J. Am. Chem. Soc.*, 2013, **135**, 4834–4839.
208 M. Zarek, N. Mansour, S. Shapira and D. Cohn, *Macromol. Rapid Commun.*, 2017, **38**, 015002.
209 M. Hippler, E. Blasco, J. Qu, M. Tanaka, C. Barner-Kowollik, M. Wegener and M. Bastmeyer, *Nat. Commun.*, 2019, **10**, 232.
210 L. Zhang, H. Liang, J. Jacob and P. Naumov, *Nat. Commun.*, 2015, **6**, 7429.
211 D. Raviv, W. Zhao, C. McKnelly, A. Papadopoulou, A. Kadambi, B. Shi, S. Hirsch, D. Dikovsky, M. Zyracki, C. Olguin, R. Raskar and S. Tibbits, *Sci. Rep.*, 2014, **4**, 7422.
212 Y. Mao, Z. Ding, C. Yuan, S. Ai, M. Isakov, J. Wu, T. Wang, M. L. Dunn and H. J. Qi, *Sci. Rep.*, 2016, **6**, 24761.
213 A. S. Gladman, E. A. Matsumoto, R. G. Nuzzo, L. Mahadevan and J. A. Lewis, *Nat. Mater.*, 2016, **15**, 413–418.
214 M. C. Mulakkal, R. S. Trask, V. P. Ting and A. M. Seddon, *Mater. Des.*, 2018, **160**, 108–118.
215 K. Zhang, J. S. Kimball, R. R. Nemani, S. W. Running, Y. Hong, J. J. Gourley and Z. Yu, *Sci. Rep.*, 2015, **5**, 15956.
216 J. C. Breger, C. Yoon, R. Xiao, H. R. Kwag, M. O. Wang, J. P. Fisher, T. D. Nguyen and D. H. Gracias, *ACS Appl. Mater. Interfaces*, 2015, **7**, 3398–3405.
217 G. Wang, L. Yao, W. Wang, J. Ou, C.-Y. Cheng and H. Ishii, presented in part at the Proceedings of the 2016 CHI Conference on Human Factors in Computing Systems – CHI '16, 2016.
218 C. Lv, H. Xia, Q. Shi, G. Wang, Y.-S. Wang, Q.-D. Chen, Y.-L. Zhang, L.-Q. Liu and H.-B. Sun, *Adv. Mater. Interfaces*, 2017, **4**, 1601002.
219 D. Lei, Y. Yang, Z. Liu, S. Chen, B. Song, A. Shen, B. Yang, S. Li, Z. Yuan, Q. Qi, L. Sun, Y. Guo, H. Zuo, S. Huang, Q. Yang, X. Mo, C. He, B. Zhu, E. M. Jeffries, F.-L. Qing, X. Ye, Q. Zhao and Z. You, *Mater. Horiz.*, 2019, **6**, 394–404.
220 H. Yang, W. R. Leow, T. Wang, J. Wang, J. Yu, K. He, D. Qi, C. Wan and X. Chen, *Adv. Mater.*, 2017, **29**, 1701627.
221 Y. Liu, B. Shaw, M. D. Dickey and J. Genzer, *Sci. Adv.*, 2017, **3**, e1602417.
222 O. Kuksenok and A. C. Balazs, *Mater. Horiz.*, 2016, **3**, 53–62.
223 X. Mu, N. Sowan, J. A. Tumbic, C. N. Bowman, P. T. Mather and H. J. Qi, *Soft Matter*, 2015, **11**, 2673–2682.
224 J. Wu, Z. Zhao, X. Kuang, C. M. Hamel, D. Fang and H. J. Qi, *Multifunct. Mater.*, 2018, **1**, 015002.
225 M. K. Gupta, F. Meng, B. N. Johnson, Y. L. Kong, L. Tian, Y. W. Yeh, N. Masters, S. Singamaneni and M. C. McAlpine, *Nano Lett.*, 2015, **15**, 5321–5329.
226 A. Miriyev, K. Stack and H. Lipson, *Nat. Commun.*, 2017, **8**, 596.
227 H. Okuzaki, T. Kuwabara, K. Funasaka and T. Saido, *Adv. Funct. Mater.*, 2013, **23**, 4400–4407.
228 Y. Kim, H. Yuk, R. Zhao, S. A. Chester and X. Zhao, *Nature*, 2018, **558**, 274–279.
229 Y. S. Lui, W. T. Sow, L. P. Tan, Y. Wu, Y. Lai and H. Li, *Acta Biomater.*, 2019, **92**, 19–36.
230 Y. Yang, X. Li, M. Chu, H. Sun, J. Jin, K. Yu, Q. Wang, Q. Zhou and Y. Chen, *Sci. Adv.*, 2019, **5**, eaau9490.
231 G. Kim and Y. M. Shkel, *J. Mater. Res.*, 2011, **19**, 1164–1174.
232 J. Wang, T. Lu, M. Yang, D. Sun, Y. Xia and T. Wang, *Sci. Adv.*, 2019, **5**, eaau8769.

